

THESIS

COMPUTATIONAL MODELING OF CADMIUM SULFIDE DEPOSITION IN THE  
CdS/CdTe SOLAR CELL MANUFACTURING PROCESS

Submitted by

Davis Robert Hemenway

Department of Mechanical Engineering

In partial fulfillment of the requirements

For the Degree of Master of Science

Colorado State University

Fort Collins, Colorado

Spring 2013

Master's Committee:

Advisor: Hiroshi Sakurai

Walajabad Sampath  
James Sites

Copyright by Davis Robert Hemenway 2013  
All Rights Reserved

## ABSTRACT

### COMPUTATIONAL FLUID DYNAMICS ANALYSIS OF CdS DEPOSITION IN THE CdTe SOLAR CELL MANUFACTURING PROCESS

A thin film CdS/CdTe solar cell manufacturing line has been developed in the Photovoltaic Materials Engineering Lab at Colorado State University. This system incorporates multiple stations using NiCr embedded heaters in graphite crucibles to successively sublime layers of different photovoltaic materials onto glass substrates. Times, temperatures and chemical compositions of these layers can be varied or excluded according to the desired characteristics of the 3" x 3" solar cell sample. Though the tool allows for flexibility and variability of materials, the uniformity of material deposition remains one of the largest sources of performance variability between samples.

Computational Fluid Dynamics (CFD) programs have been used previously to predict the thermal performance of the embedded heaters and to ensure thermal uniformity in each of the heated deposition pockets. The thermal modeling used in the designing of these sources has been proven to be within 2.5% of the experimentally measured temperatures in laboratory and industrial applications.

Building off of the thermal modeling effort, CFD models were created to model the sublimation, vapor transport and film deposition that occurs within the CdS source. Fluid models of the CdS source were created to accurately reflect the current deposition technique with the intent of predicting future deposition uniformity during the evaluation process for new source designs. The developed model was able to accurately predict film growth in an untested source in

which the uniformity of the film deposition was increased by over 70%. These models were created using ANSYS Fluent, and utilized Arrhenius reaction rate equations to describe the sublimation and condensation reactions. Modeling results showed a strong correlation with the experimental data.

## ACKNOWLEDGEMENTS

I would first and foremost like thank God for blessing me with a supportive family. As a civil engineer, my father began teaching me at a young age to think logically and critically about the world around me. My mother always fostered my education and taught me discipline in my studies. Without either of them, I would not be the man I am today. I would also like to thank my brother and sisters for always challenging and sharpening me and my fiancée for supporting me throughout my graduate career.

I would like to acknowledge my graduate committee and the influence they have had on this research: Dr. Sakurai for freely giving of his and expertise on computational methods and techniques, Dr. Sampath for sharing his absolute passion for advancing the entire field of CdS/CdTe devices and photovoltaics, and Dr. Sites for his knowledge of PV device physics and performance. Thanks also to everyone in the Photovoltaic Material Engineering Lab for their hard work, flexibility and willingness to assist me in my research. Specifically, I would like to mention Kevan Cameron, who assisted me with creating samples for testing and kept our lab running smoothly. Also, thanks to Kevin Walters, Jason Kephart, Pavel Kobayakov, and Drew Swanson, whom all gave me advice and support whenever it was needed.

Finally, I would like to thank Jack Clark from Surface Analytics LLC and Kurt Barth from Abound Solar Inc. Mr. Barth was instrumental in keeping me on schedule and without Mr. Clark's assistance with Scanning White Light Interferometry; this research would not have been possible.

# TABLE OF CONTENTS

ABSTRACT.....	ii
ACKNOWLEDGEMENTS.....	iv
TABLE OF CONTENTS.....	v
CHAPTER 1: INTRODUCTION.....	1
1.1 THE CURRENT STATE OF GLOBAL ENERGY CONSUMPTION.....	1
1.2 THIN FILM CDS/CDTE SOLAR CELL DESIGN.....	6
1.3 PROJECT MOTIVATION.....	7
1.4 FUTURE IMPROVEMENTS TO CDS/CDTE DEVICE PERFORMANCE.....	8
CHAPTER 2: EXPERIMENTAL METHODS.....	13
2.1 CLOSE-SPACE SUBLIMATION METHOD.....	13
2.2 ADVANCED RESEARCH DEPOSITION SYSTEM.....	15
2.3 SAMPLE PREPARATION AND ANALYSIS.....	18
CHAPTER 3: MODELING CONSIDERATIONS.....	24
3.1 MOTIVATION.....	24
3.2 FLUID MECHANICS THEORY.....	25
3.3 HEAT TRANSFER THEORY.....	27
3.4 CHEMICAL REACTION THEORY.....	30
3.5 COMPUTATIONAL RESOURCES.....	34
CHAPTER 4: CHEMICAL REACTION RATE MODEL.....	35
CHAPTER 5: PREDICTING FILM GROWTH IN AN ALTERNATIVE SOURCE.....	42
5.1 MOTIVATION.....	42
5.2 DESCRIPTION OF THE MODIFIED SOURCE.....	42
5.3 RESULTS.....	45
CHAPTER 6: DISCUSSION AND FUTURE WORK.....	55
6.1 DISCUSSION OF RESULTS.....	55
6.2 COMBINED THERMAL AND FLUID MODELING.....	55
6.3 FUTURE WORK.....	58
REFERENCES.....	61

## LIST OF FIGURES

Figure 1. US 2011 energy flow (Quadrillion Btu) [5] .....	1
Figure 2. Average daily sunshine (kW/m <sup>2</sup> ) [7] .....	2
Figure 3. Regional PV cell and module shipments, 2000-2010 [8].....	2
Figure 4. US annual installed grid-connected PV capacity by market 2001-2010 [8] .....	3
Figure 5. Price of photovoltaic power 1989-2010 (\$/W).....	3
Figure 6. Laboratory best-cell efficiencies for various PV technologies [8].....	4
Figure 7. Manufacturing cost per watt for various PV technologies [10] .....	5
Figure 8. Module costs of CdTe and silicon solar devices[11].....	5
Figure 9. Basic CdTe device structure .....	6
Figure 10. Raw material cost per watt of different PV materials [1].....	7
Figure 11. A source fitted with PECSS .....	9
Figure 12. Stacked source CMT co-sublimation .....	10
Figure 13. Side-by-side CMT co-sublimation .....	11
Figure 14. Current and future cell design .....	12
Figure 15. CdS film thickness after a 110 second deposition.....	14
Figure 16. Overview of the ARDS .....	15
Figure 17. Stations 1-4 in the ARDS .....	16
Figure 18. Graphite source geometry.....	17
Figure 19. Deposition station assembly .....	18
Figure 20. Graphite source geometry: Substrates enter from right side of source .....	18

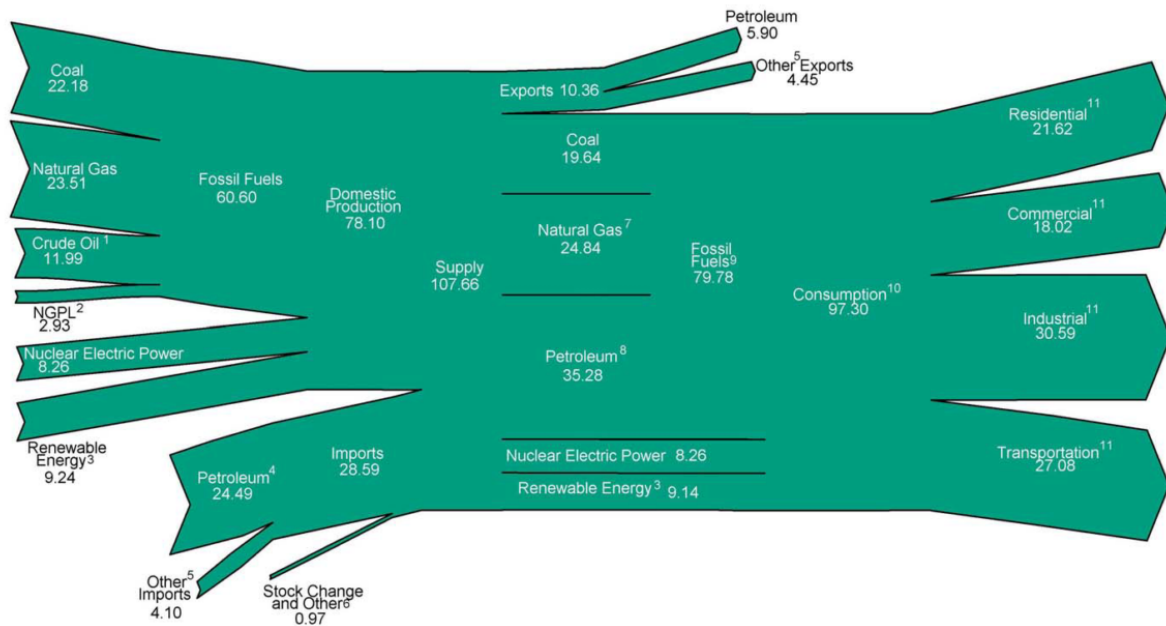
Figure 21. An etched CdS film .....	20
Figure 22. Optical configuration of dispersive white-light interferometry; LP: linear polarizer, BS: beam splitter, PBS: polarizing beam splitter, ES: entrance slit, DG: dispersive grating, CCD: charge coupled device [41] .....	22
Figure 23. A typical SWLI image.....	23
Figure 24. Measurement of the step height from SWLI data .....	23
Figure 25. Radiative heat transfer through a fluid volume [52] .....	29
Figure 26. Molecular motion in the fluid volume of the pocket.....	34
Figure 27. 3D chemical rate model: Cd molar fraction in the source.....	36
Figure 28. 3D chemical rate model: Deposition rate of Cd on the substrate (kg/m <sup>2</sup> -s) .....	38
Figure 29. Film thickness across the substrate: Chemical reaction rate source.....	38
Figure 30. 3D chemical rate model: Temperature in the pocket (K).....	39
Figure 31. 3D chemical rate model: Incident radiation in the pocket (w/m <sup>2</sup> ).....	40
Figure 32. 3D chemical rate model: Incident radiation on the CdS source surface (w/m <sup>2</sup> ).....	41
Figure 33. 3D chemical rate model: Incident radiation on the substrate (w/m <sup>2</sup> ) .....	41
Figure 34. Normal graphite source geometry: With end effector .....	44
Figure 35. Modified source geometry.....	44
Figure 36. Modified source mesh .....	45
Figure 37. Modified source model: Local CdS deposition rates overlaid with approximate SAD locations on the substrate .....	46
Figure 38. 3D chemical reaction rate model: Local CdS deposition rates overlaid with approximate SAD locations on the substrate .....	47
Figure 39. Normal source: Pathlines colored by velocity magnitude (m/s) .....	48

Figure 40. Modified source: Pathlines colored by velocity magnitude (m/s).....	48
Figure 41. Modified source: Cd molar fraction in the source.....	49
Figure 42. Normal source: Cd molar fraction in the source .....	50
Figure 43. Modified source: Incident radiation on the CdS source surface (w/m <sup>2</sup> ).....	51
Figure 44. Modified source: Incident radiation on the CdS source surface (w/m <sup>2</sup> ).....	51
Figure 45. Film thickness across the substrate: Modified source .....	53
Figure 46. 2D thermal and fluid model: Geometry.....	56
Figure 47. 2D thermal and fluid model: Temperature in the source (K).....	56
Figure 48. Simple 3D thermal and fluid model: Geometry .....	57
Figure 49. Simple 3D thermal and fluid model: Temperature in the source (K).....	57
Figure 50. Comprehensive 3D thermal and fluid model: Geometry .....	58

## CHAPTER 1: INTRODUCTION

### 1.1 The Current State of Global Energy Consumption

On a global scale, annual energy consumption is around 17,000 Terawatt-hours (TWh) per year. The United States alone utilizes 4,000 TWh of energy each year [1]. Around 80% of the energy utilized internationally comes from petroleum, natural gas and coal, all traditionally considered fossil fuels [2]. Though renewable energy sources have been around for decades, they are responsible for producing only 3.4% of the total energy consumed globally [3]. As worldwide energy consumption is predicted to increase as much as 50% by 2035 [4], there is concern that fossil fuel sources will not be viable due to diminishing supplies and environmental impact.



<sup>1</sup> Includes lease condensate.

<sup>2</sup> Natural gas plant liquids.

<sup>3</sup> Conventional hydroelectric power, biomass, geothermal, solar/photovoltaic, and wind.

<sup>4</sup> Crude oil and petroleum products. Includes imports into the Strategic Petroleum Reserve.

<sup>5</sup> Natural gas, coal, coal coke, biofuels, and electricity.

<sup>6</sup> Adjustments, losses, and unaccounted for.

<sup>7</sup> Natural gas only; excludes supplemental gaseous fuels.

<sup>8</sup> Petroleum products, including natural gas plant liquids, and crude oil burned as fuel.

<sup>9</sup> Includes 0.01 quadrillion Btu of coal coke net imports.

<sup>10</sup> Includes 0.13 quadrillion Btu of electricity net imports.

<sup>11</sup> Total energy consumption, which is the sum of primary energy consumption, electricity retail sales, and electrical system energy losses. Losses are allocated to the end-use sectors in proportion to each sector's share of total electricity retail sales. See Note, "Electrical Systems Energy Losses," at end of Section 2.

Notes: • Data are preliminary. • Values are derived from source data prior to rounding for publication. • Totals may not equal sum of components due to independent rounding.  
Sources: Tables 1.1, 1.2, 1.3, 1.4, and 2.1a.

Figure 1. US 2011 energy flow (Quadrillion Btu) [5]

Recently, there has been a global trend of increasing renewable energy sources such as solar, wind and hydroelectric. Solar energy in particular has become attractive due to the amount of energy available and the areas in which it can be easily collected. More solar energy falls on the Earth than all other renewable energy sources combined [6]. Because of this, the production of photovoltaic modules has increased along with the cumulative installed PV capacity.

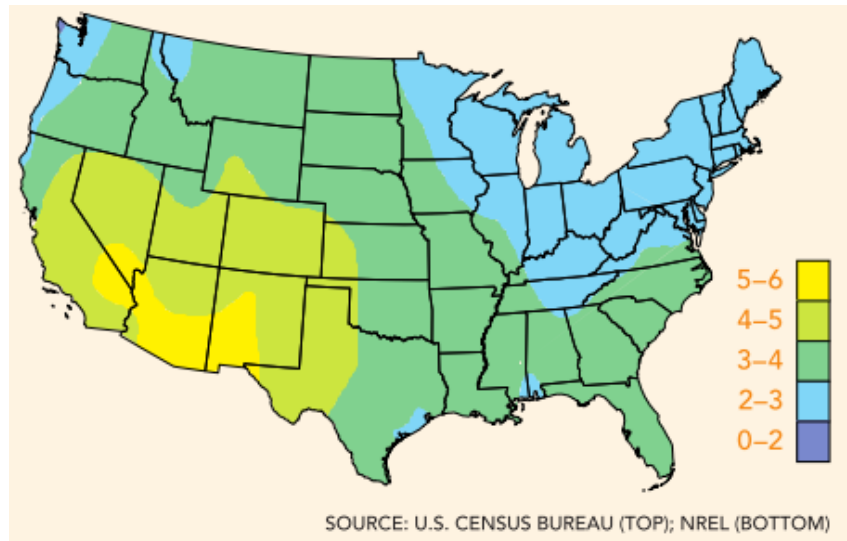


Figure 2. Average daily sunshine (kW/m<sup>2</sup>) [7]

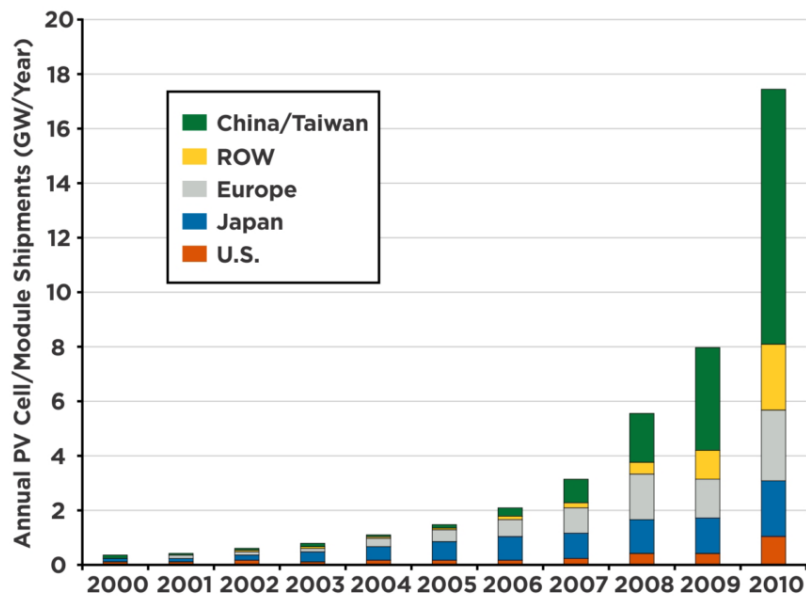


Figure 3. Regional PV cell and module shipments, 2000-2010 [8]

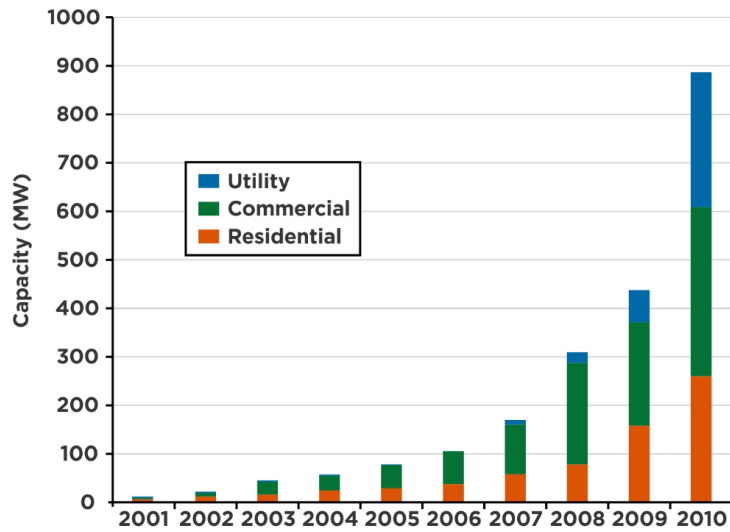


Figure 4. US annual installed grid-connected PV capacity by market 2001-2010 [8]

The future of photovoltaic electricity is bright. As gains are made in module efficiency and manufacturing costs decrease, the overall cost per watt of photovoltaic power has steadily decreased. The US Department of Energy has recently instituted the SunShot initiative, the end goal of which is to reduce the installed cost per watt of PV power below \$1/Watt. It is at this price, that purchasing PV power is thought to be economically feasible for large scale implementation.

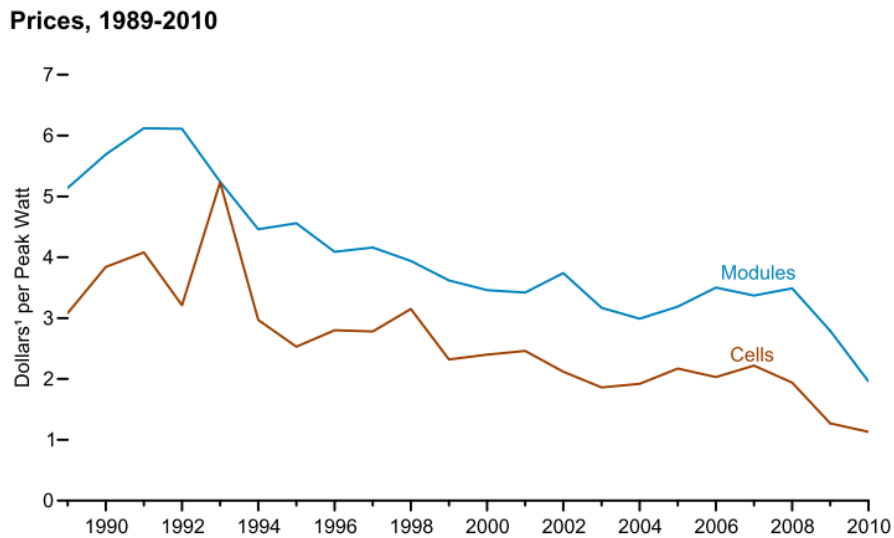


Figure 5. Price of photovoltaic power 1989-2010 (\$/W)

The photovoltaics industry has traditionally been dominated by crystalline silicon devices however; thin film devices, such as CIGS and CdTe, have begun to take significant portions of the market share [9]. Of these two thin film technologies, CdTe has proven to be the most economically feasible, even beating crystalline silicon in installed cost per watt for large installations.

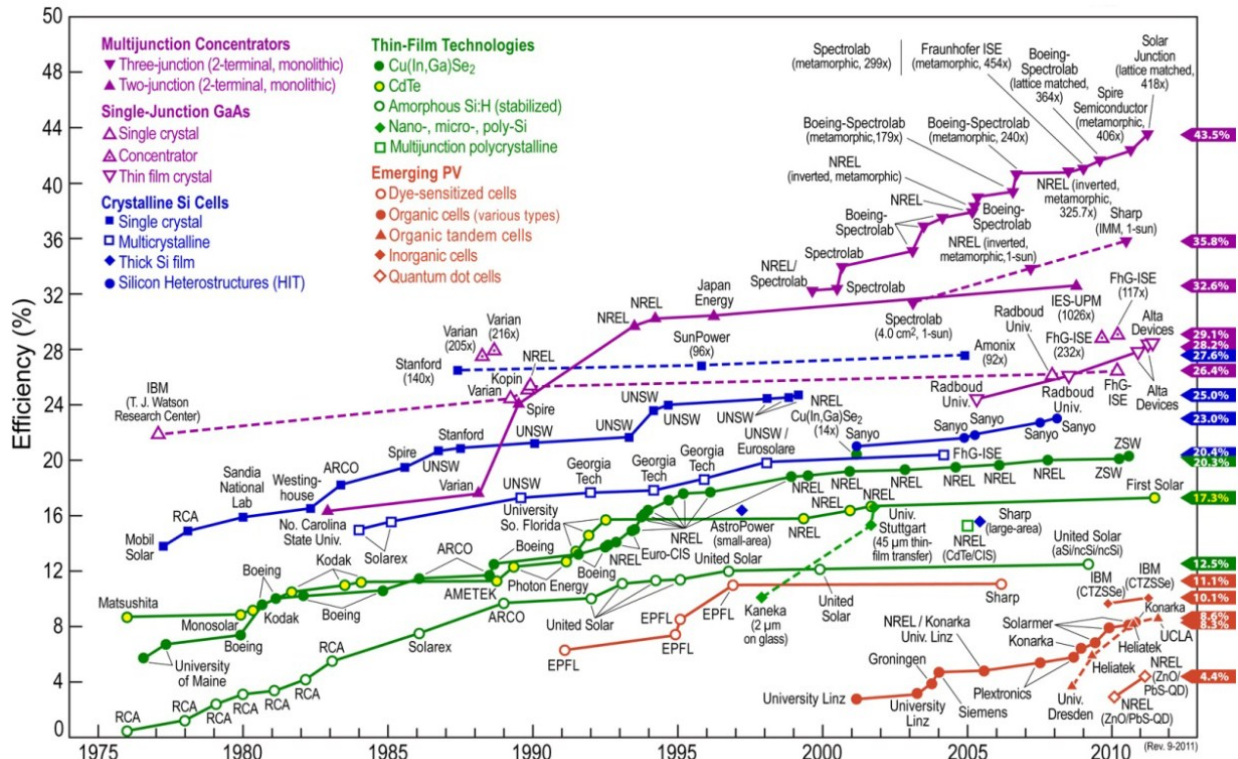


Figure 6. Laboratory best-cell efficiencies for various PV technologies [8]

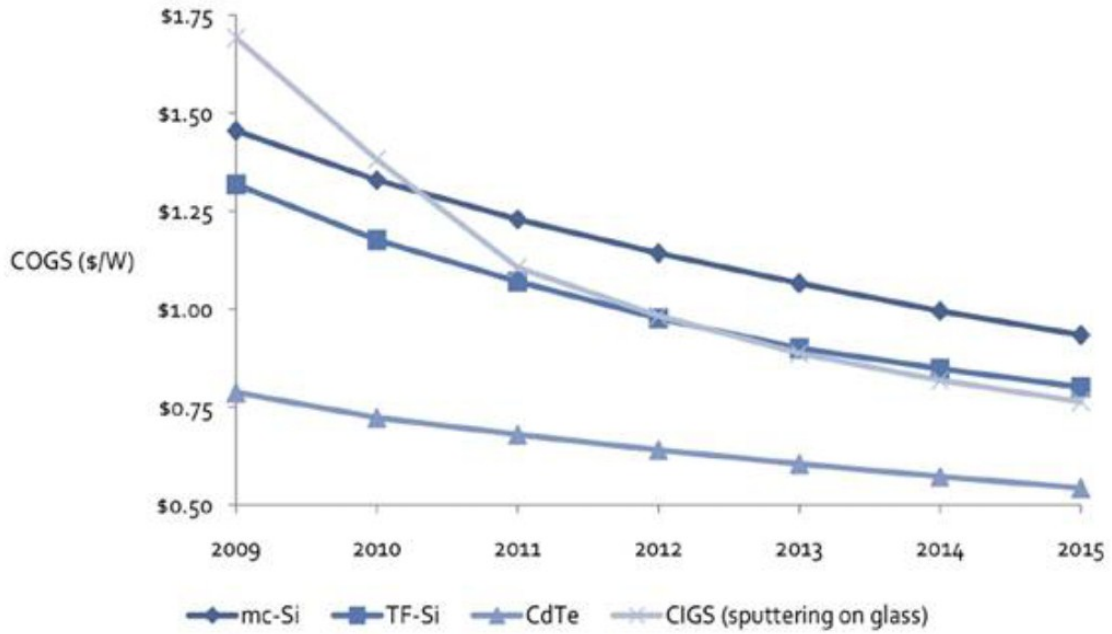


Figure 7. Manufacturing cost per watt for various PV technologies [10]

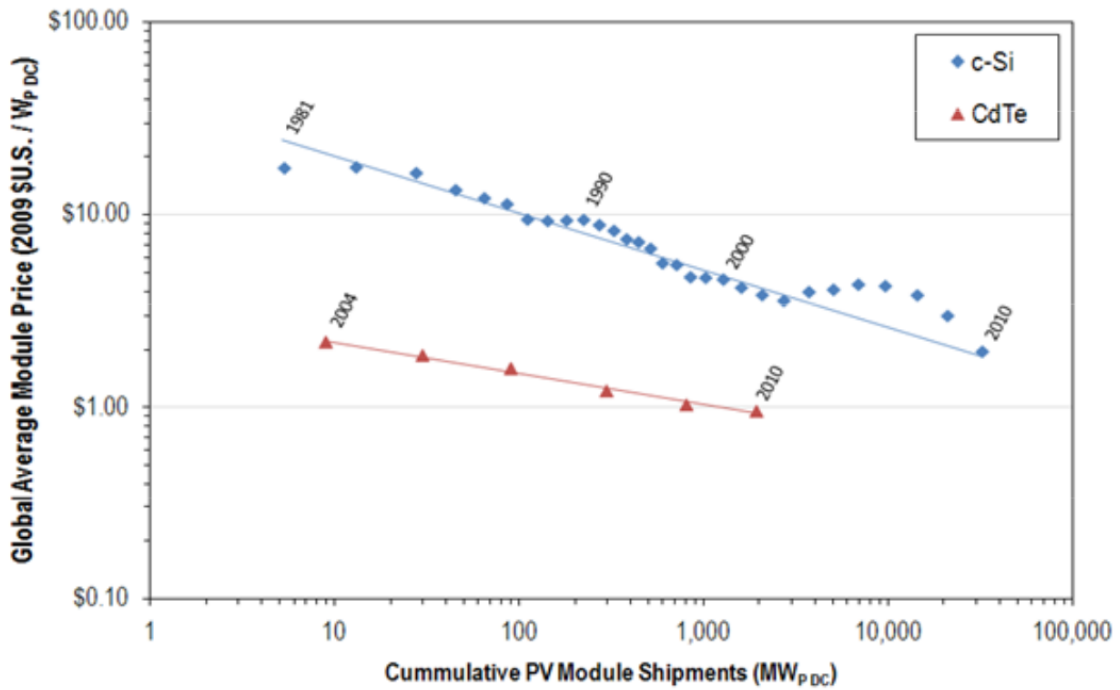


Figure 8. Module costs of CdTe and silicon solar devices[11]

## 1.2 Thin Film CdS/CdTe Solar Cell Design

The typical CdS/CdTe device is a p-n heterojunction photodiode. CdS/CdTe solar cells employ a superstrate structure on highly transparent glass to achieve high efficiencies. The glass is sequentially coated with a transparent conducting oxide (TCO) layer, CdS as a window layer, CdTe as an absorber layer, and is then covered with a back contact [12].

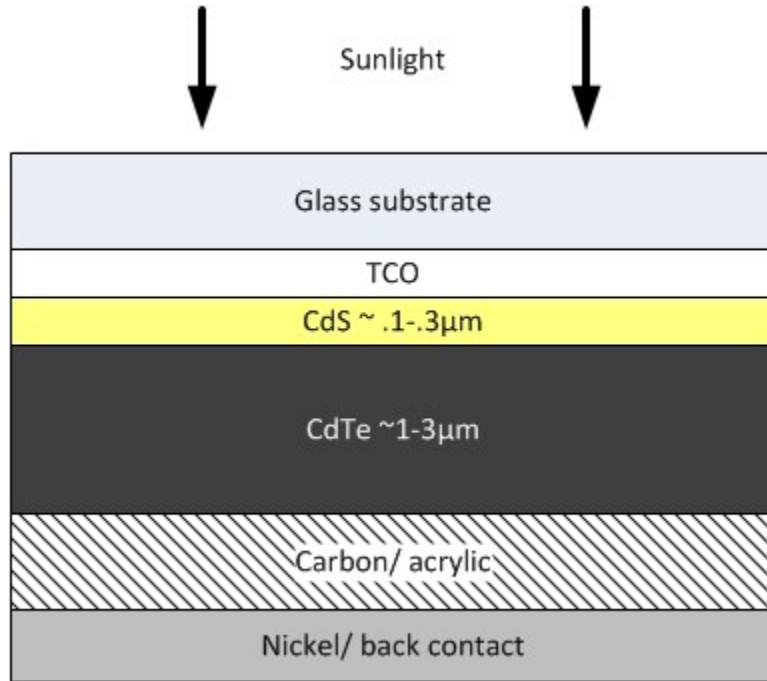


Figure 9. Basic CdTe device structure

There are many compounds available that can be employed as a window layer; however, many manufacturers use CdS for a number of reasons [13]. CdS is a widely used II-VI compound semiconductor that has been employed in several electrical and even biological applications [14–16]. Because of this, the electrical and optical properties of CdS are universally understood to be suitable for pairing with CdTe for thin-film photovoltaic applications. CdS has excellent transmission in the visible range [17], [18], low resistivity [19], and a band gap near 2.42eV [20]. Another large reason why CdS is continually utilized is because it is a comparatively inexpensive photovoltaic material, as seen in Figure 10.

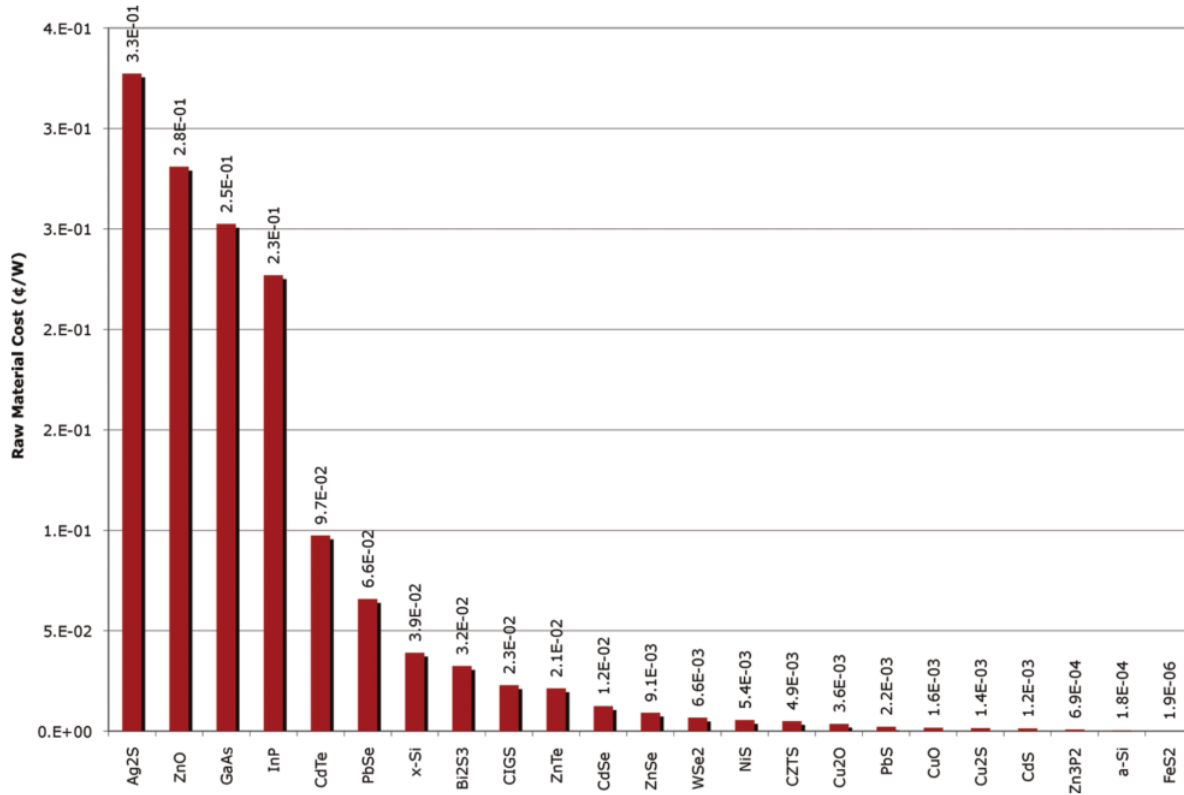


Figure 10. Raw material cost per watt of different PV materials [1]

### 1.3 Project Motivation

As the solar industry becomes increasingly competitive, cost per watt is a metric that is often used by customers to gauge the feasibility of installing solar panels. CdS/CdTe solar cell producers must make high-efficiency cells with low manufacturing costs to remain profitable. Several techniques have been utilized to create thin film CdS/CdTe solar cells, including metal organic chemical vapor deposition [21], hot wall epitaxy [22], hot-wall flash evaporation [23], screen printing [24], chemical bath deposition [25], physical vapor deposition, sputtering, and close-space sublimation [26].

Close space sublimation (CSS) has shown promising results as method for the efficient, large-scale manufacturing of thin film CdS/CdTe solar cells [27], [28]. In industrial

environments, this method has proven to be one of the most rapid ways of depositing high-purity thin films [29]. Companies such as Abound Solar have used CSS as a manufacturing technique to create 2'x4' panels from incoming glass to shipping crate in approximately 2.5 hours [30].

Despite their success with the rapid production of large photovoltaic devices, many CSS CdS/CdTe device manufacturers struggle with uniform film deposition. Film uniformity is paramount to overall module performance, especially the CdS window layer [31]. Areas of thin CdS can increase the short-circuit current of the module but can also lead to low voltage and low fill factors. With a uniform window layer, the thickness can be properly varied to achieve the desired device parameters. One such device parameter that varies with the thickness of the CdS film is the series resistance [32], [33]. Also, without uniform layers, CdCl<sub>2</sub> and heat treatments affect areas of the device non-uniformly and cannot be optimized for the entire module.

At Colorado State University, computational fluid dynamics (CFD) modeling has recently been utilized to better understand the deposition process for the CdS window layer. This type of analysis was chosen so that the film deposition of unique, three-dimensional sources could be investigated and used to accurately predict film uniformity in future source designs. By evaluating the film uniformity of a source before it is manufactured, companies and researchers will be able iteratively optimize designs so that highly uniform films can be manufactured without wasting time and money on poor source designs or costly prototypes.

#### *1.4 Future Improvements to CdS/CdTe Device Performance*

The vast majority of research in the field of CdTe solar devices revolves around increasing the overall efficiency. At the Photovoltaic Materials Engineering Laboratory (PVMEL) at Colorado State University, there are currently several avenues of research being pursued to

increase the efficiency such as incorporating plasma into the manufacturing process, sputtering CdS with oxygen to increase transparency, and applying a  $Cd_{1-x}Mg_xTe$  electron reflector on the back surface.

Plasma research at the VMEL is currently concentrated on substrate cleaning and Plasma Enhanced Close-Space Sublimation (PECSS). In the field of plasma cleaning, recent experiments have shown that by exposing the substrate to  $N_2-O_2$  plasma after cleaning it using traditional methods, the amount of “pinholes” is greatly reduced. Pinholes and other film defects can negatively affect overall cell efficiency. The other area of plasma research at the VMEL has been PECSS, in which plasma is created in the deposition pocket. The intended benefit that this may produce is a more uniform deposited layer and incorporating nitrogen, oxygen or other molecules that may be in the plasma. By doping films with different molecules, specific, desired band gaps or transparencies can be achieved. This process also helps to increase the adhesion between layers. Displayed in Figure 11, A is the plasma power supply and B is the vapor feed.

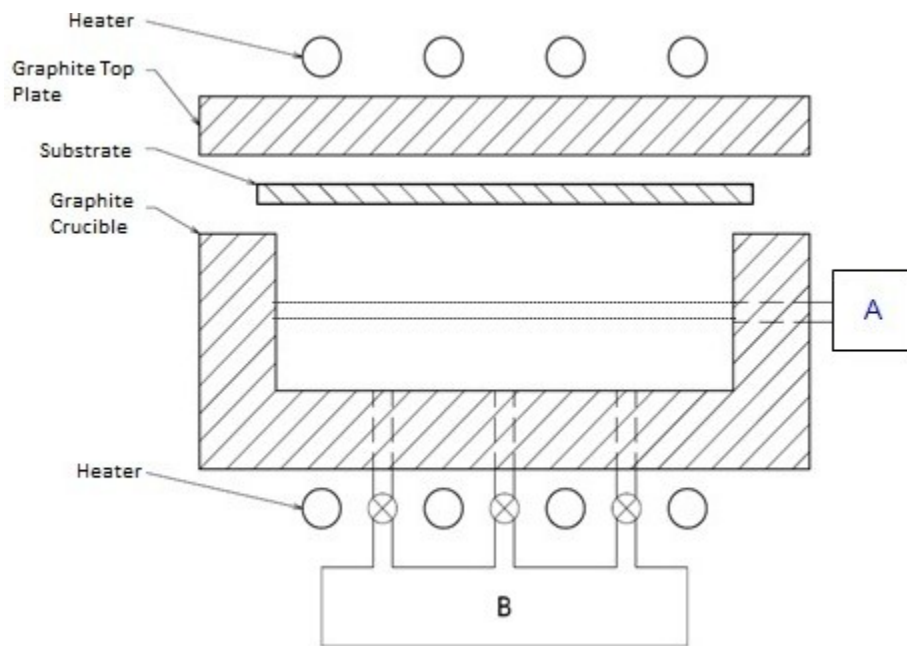


Figure 11. A source fitted with PECSS

Another large area being explored for efficiency gains is the addition of a  $\text{Cd}_{1-x}\text{Mg}_x\text{Te}$  (CMT) electron reflector. Electron reflectors work by creating a very high band gap material that prevents electrons from recombining on the back contact but instead reflects electrons back into the absorbing CdTe layer. By absorbing more electrons, the overall efficiency of the cell can theoretically be increased by 3-4%. CMT is being researched because the grain structure is similar to that of the underlying CdTe and it can be added using the same close space sublimation method with only a few modifications. The current methods of depositing such an electron reflector are sublimation through stacked sources, and sublimation from two separate “point sources”. When stacked sources are utilized, a more controllable and even deposition is made but if conditions are not held precisely, the sublimating Mg can form an oxide on the CdTe source and stop it from sublimating. The side-by-side co-sublimation method can be used to prevent this, but a graded, uneven deposition is obtained.

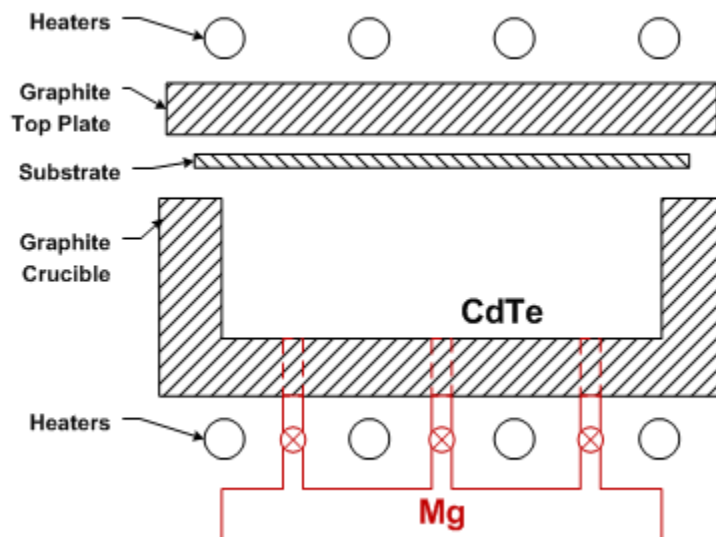


Figure 12. Stacked source CMT co-sublimation

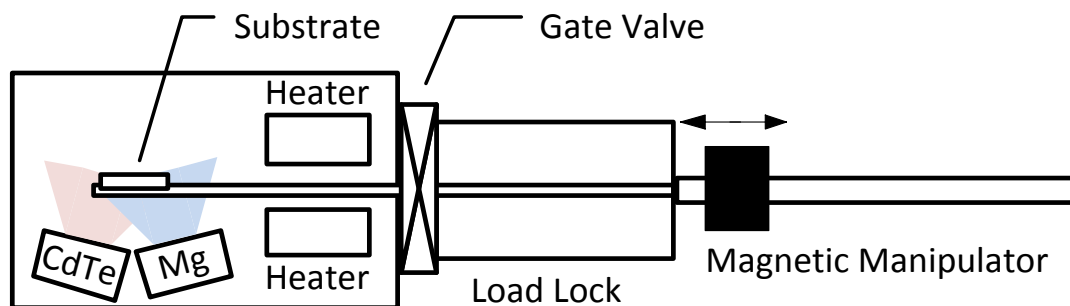


Figure 13. Side-by-side CMT co-sublimation

Sputtering CdS with oxygen and multi-junction cells are other fields of investigations for increasing solar cell efficiency. By sputtering CdS in plasma containing small amounts of oxygen, the transparency of the window layer is increased which lets more photons through to the CdTe layer. Recent samples have shown that by simply making this layer more transparent, the cell may become a full percent more efficient. Incorporating these improvements into a multi-junction cell is also in the future of CdTe. The theoretical limit of the efficiency that can be obtained using a single-junction solar cell is 40.7%, but by adding several junctions with different band gaps, the overall efficiency that can be attained is 86.8% [34]. Below is the roadmap of the Next Generation Photovoltaics I/UCRC to pursue higher efficiency through incorporation of sputtered Cd and multiple-junction cells.

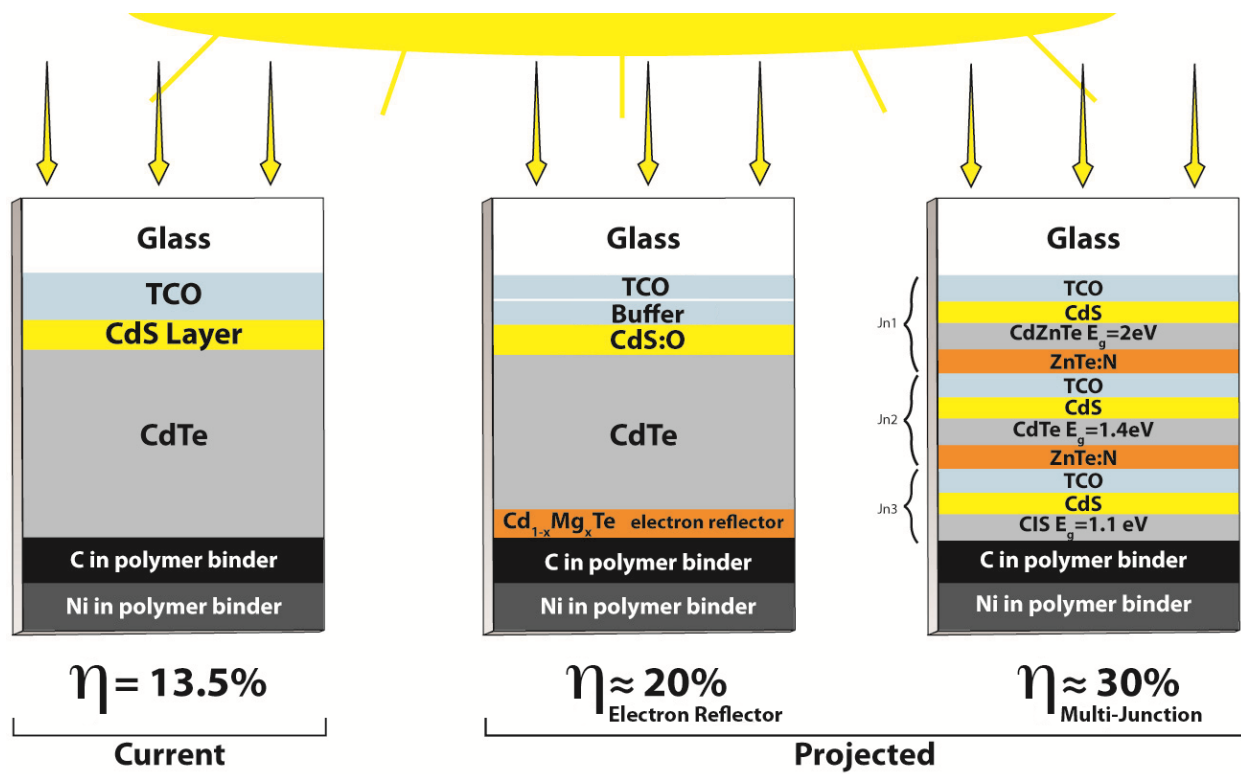


Figure 14. Current and future cell design

The bulk of other research efforts focus on different manufacturing techniques and the utilization of alternative substrates.

## CHAPTER 2: EXPERIMENTAL METHODS

### 2.1 *Close-Space Sublimation Method*

For the manufacturing of thin film CdS/CdTe solar cells in the PVMEEL, a close space sublimation technique is utilized. The term close space sublimation refers to the evaporation and deposition of some material from a heated source to a substrate in a vacuum. The distance between source and substrate can be anywhere from a few millimeters to a few inches. These reactions lead to the relatively rapid deposition of high-purity polycrystalline films. Compared to other deposition techniques, CSS is characterized by high transport efficiency, simple deposition, easily achievable vacuum pressures, and moderate temperatures.

The two factors that most affect deposition rates in CSS manufacturing environments are the operating temperatures and pressures. For a given pressure, the source temperature is the largest contributing factor to the rate of film growth [35–37]. Higher source temperatures correlate with higher deposition rates due to more photovoltaic material molecules being heated above the sublimation temperature. Substrate temperature also plays a role in the rate of deposition that can be achieved using CSS. Experiments suggest that for many thin films, such as CdTe, there exists a certain substrate temperature, up to which, the growth rate is relatively constant. However above this breakpoint temperature, as the evaporation losses on the substrate become more dominant, the growth rate is highly temperature dependent due to the surface kinetics of adsorption, formation and evaporation.

Previous work for CdTe had determined that in the pressure regime in which the ARDS operates, the growth rate is sublimation limited [36]. The assumption before modeling began was that the growth of CdS was also sublimation limited and that small changes in pressure

would not affect the deposition rate. However, in experiments performed in the ARDS, the deposition rate of CdS in CSS showed a strong linear dependence on the pressure (Figure 15).

These results indicate that the sublimation and deposition processes are diffusion limited rather than sublimation limited. In the sublimation limited case, fluid mechanics are not taken into account and the sublimating Cd and S<sub>2</sub> molecules are assumed to “beam” directly from the source to the substrate without interacting with other molecules in the pocket. For this condition, only the view factor of the sublimating material and the substrate, along with pocket geometry dictate fluid motion and film deposition uniformity. However, in the diffusion-limited case, fluid motion is characterized by the Navier-Stokes equation rather than source shape. Pressure differences, species concentrations, and thermal gradients must be taken into account to accurately describe the motion and chemical composition of the fluid in the pocket.

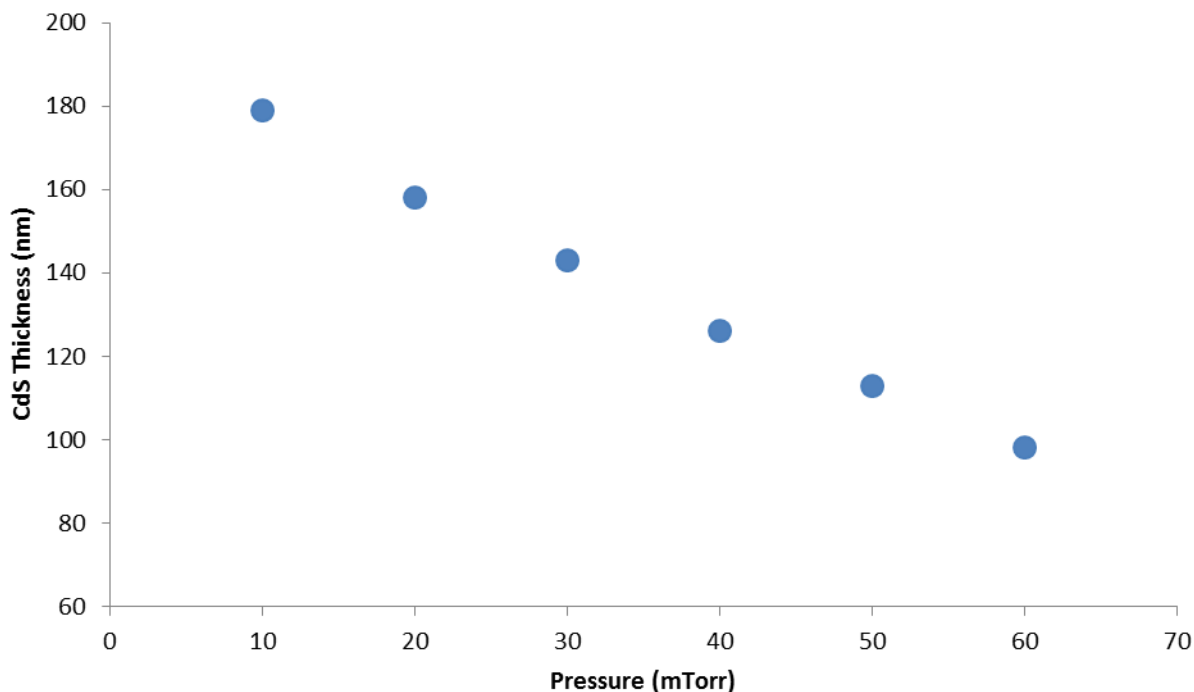


Figure 15. CdS film thickness after a 110 second deposition

## 2.2 Advanced Research Deposition System

In the PVMEEL, the majority of solar cell samples are created in a tool called the Advanced Resource Deposition System (ARDS). The tool was created to allow researchers the flexibility to fabricate CdS/CdTe cells while being able to vary deposition times, temperatures and chemistries. All of these cells are created using the CSS method by moving a small substrate over consecutive sublimating sources to deposit successive layers in a completely in-line process.

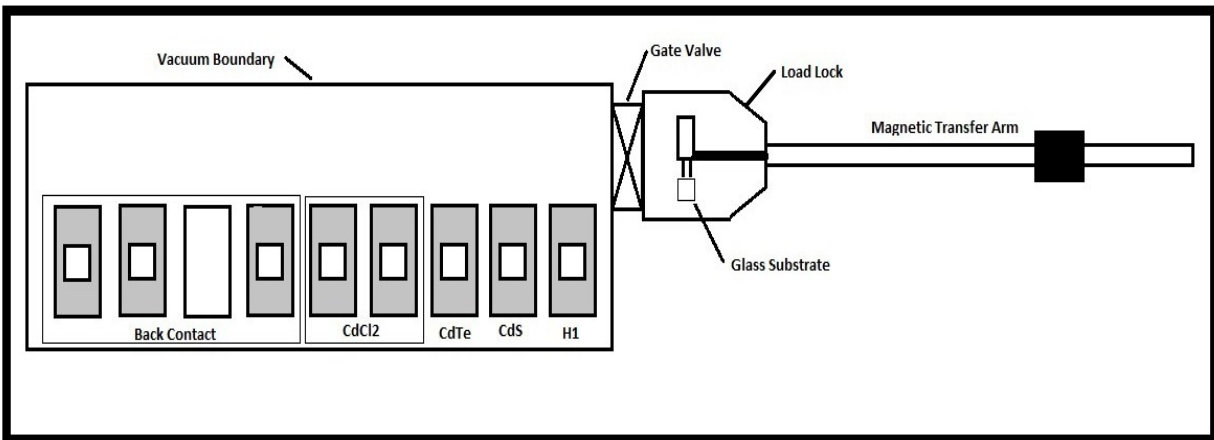


Figure 16. Overview of the ARDS

The ARDS consists of two sections separated by a gate valve: the load lock and the main chamber. In the load lock, the solar cells can be manually manipulated. This section can be vented and opened, allowing for the placement of substrates or the removal of substrates after manufacturing. After a substrate is placed in the load lock, a vacuum is created to match the pressure of the main chamber, using a Leybold D65 rotary vane pump. When the pressures are equal, the gate valve opens, allowing the substrate to move into the main chamber. Most operation within the main chamber occurs at 40mTorr with an operating gas composed of 98% nitrogen and 2% oxygen. This pressure is reached with a Leybold D65 rotary vane pump in conjunction with a Varian VHS-4 diffusion pump.



Figure 17. Stations 1-4 in the ARDS

Substrates are typically Tec-10 glass made by Pilkington, coated in a TCO layer. The substrates are received with the TCO layer already applied because most glass manufacturers have optimized this process and are readily able to supply this upon request. At the start of the deposition process, the substrate is placed TCO-side down on the end effector in the load lock. The end effector is a machined piece of Inconel that carries the substrate into the chamber and between sources. After entering the main chamber, the first station that the substrates are placed in is a heat treatment process. Top and bottom sources emit radiation, bringing the substrate to around 450°C in 110 seconds. This temperature is checked using an IR laser as the substrate moves between the first and second station.

Each source, with the exception of the two heating stations, has geometry similar to that shown in Figure 18 and Figure 20. Sources are machined from Poco 2020 Graphite, a highly thermally conductive material. A resistive Nickel-Chromium heating element is embedded in

the source and potted in the source with a ceramic that has similar properties to the graphite. As electrical current is run through the NiCr wires, the temperature in the source is monitored by a thermocouple embedded in the graphite, and controlled using a PID controller. Deposition temperatures vary by the photovoltaic material that is to be deposited. The same heating technique is utilized by the top source to ensure that the substrate maintains the correct temperature throughout the deposition process.

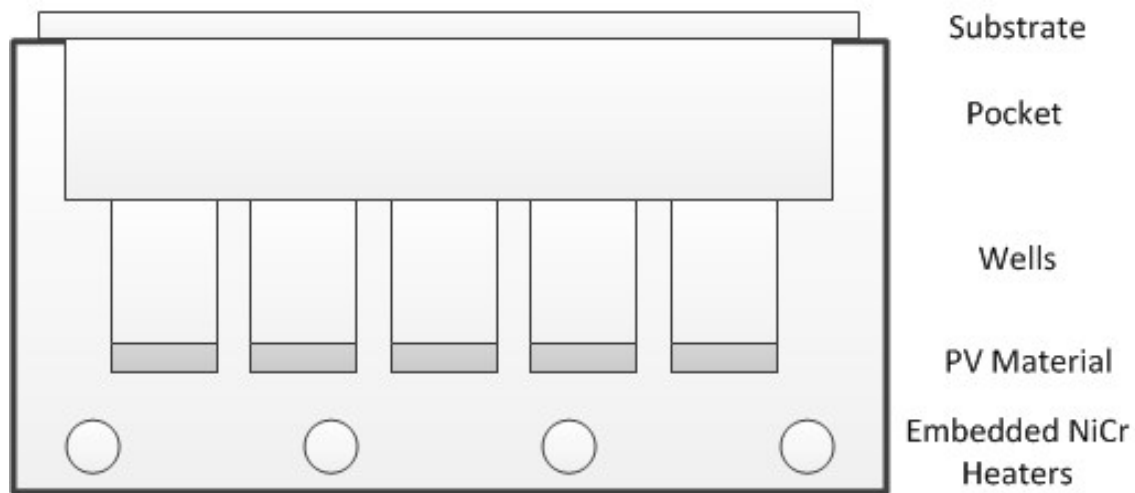


Figure 18. Graphite source geometry

For every photovoltaic material that is deposited, the CSS technique is utilized. The embedded NiCr heating element is powered until the source reaches the desired temperature for each material, causing the material to sublime at a specific rate. The substrate is held over each source for a precise amount of time, typically on the order of two minutes, until the anticipated film thickness is reached. Researchers are typically able to test fully functional devices within 45 minutes of loading a substrate onto the end effector.

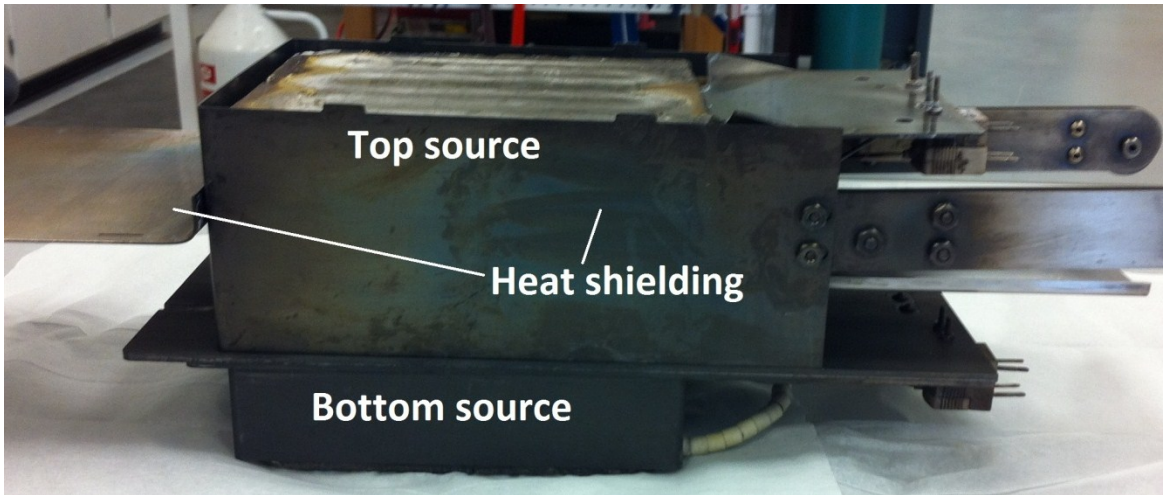


Figure 19. Deposition station assembly

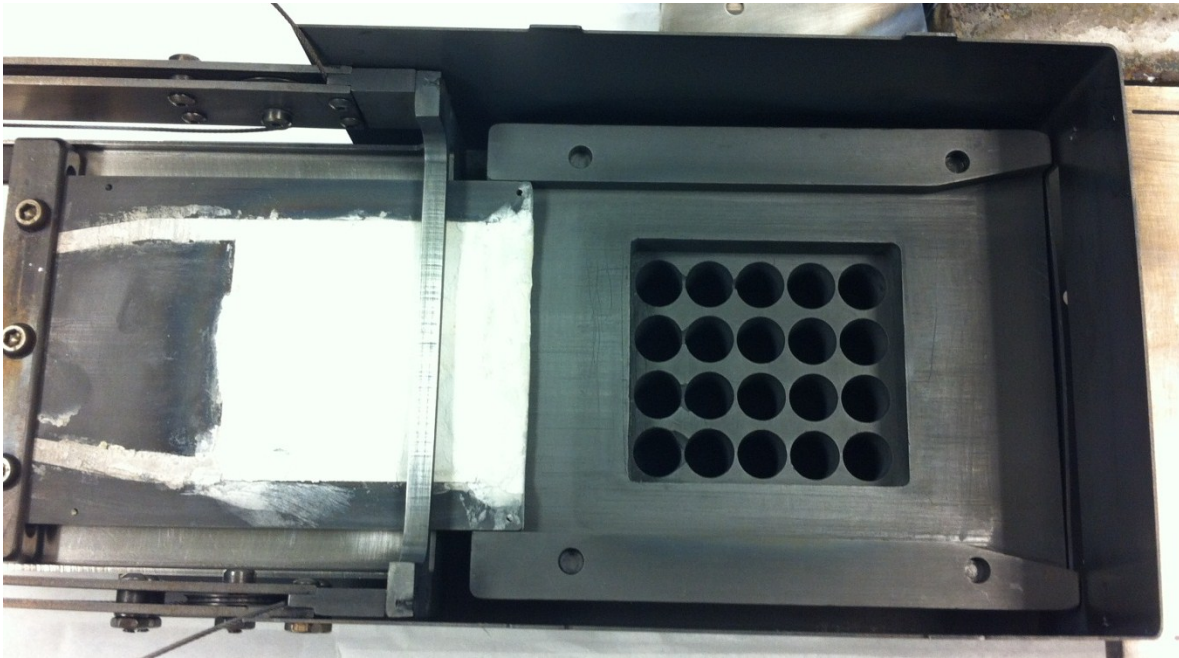


Figure 20. Graphite source geometry: Substrates enter from right side of source

### 2.3 *Sample Preparation and Analysis*

Experimental validation is an integral part of creating accurate computational models as every model makes a number of assumptions, some of which can be tested. Making correct suppositions exponentially increases the overall accuracy of the model; therefore testing and

reducing the number of unknowns within a model is imperative. At the PVMEL, much of the thermal CFD modeling effort has already been validated. IR cameras, lasers and thermocouples have all been used to extract real-time data from the sources to ensure that the predicted temperatures in the source and on the substrate are close to experimental data.

This same level of validation is needed for the fluid and film deposition modeling; however, it is much more difficult. Many parameters, such as the pressure, species concentrations and radiation intensity within the pocket, cannot be accurately measured without damaging the functionality of the deposition source itself. Currently, the PVMEL lacks the capability to measure several of these important factors. Because of this, much of the validation for the modeling came from measuring the thickness of the film across the substrate and comparing it to the predicted values.

Experimental CdS film samples were created in the ARDS at process of record (POR) conditions. The substrate was heated to around 450°C in the first station and then moved over the CdS source for 110 seconds. The bottom CdS deposition source was held at 610°C while the top source was held at 420°C. After this step, the substrates were allowed to cool and removed from the ARDS.

It was determined that to get the most complete picture of the thickness profile across the substrate, the film would need to be masked and etched across the diagonal to get “step height” values in areas of interest. The region of the substrate where the thickness diminishes was of particular interest. “Step heights” can be evaluated by measuring the height difference between areas with film and areas without film. There must be a distinct, clear difference in thicknesses of two regions for an effective measurement to be taken, so the film was masked with electroplating tape, and the rest of the film was removed with hydrochloric acid. This process

removes the CdS but leaves the TCO intact, so the measured step heights are of the CdS film alone. Also, by determining the step heights, rather than simply dragging a profilometer across the film and looking at the profile, the distortion of the glass is removed from the measurement. The glass substrate warps by a few micrometers due to the temperatures encountered in the deposition process. Since the CdS film is on the order of 100 nanometers, less than a tenth of the amount that the glass bows, a distortion of even one micrometer would invalidate the measurements. Taking step height values ensures that if the glass bows, the film moves with it and the film alone is measured- for this reason steps heights were chosen to experimentally represent the thickness values across the substrate.

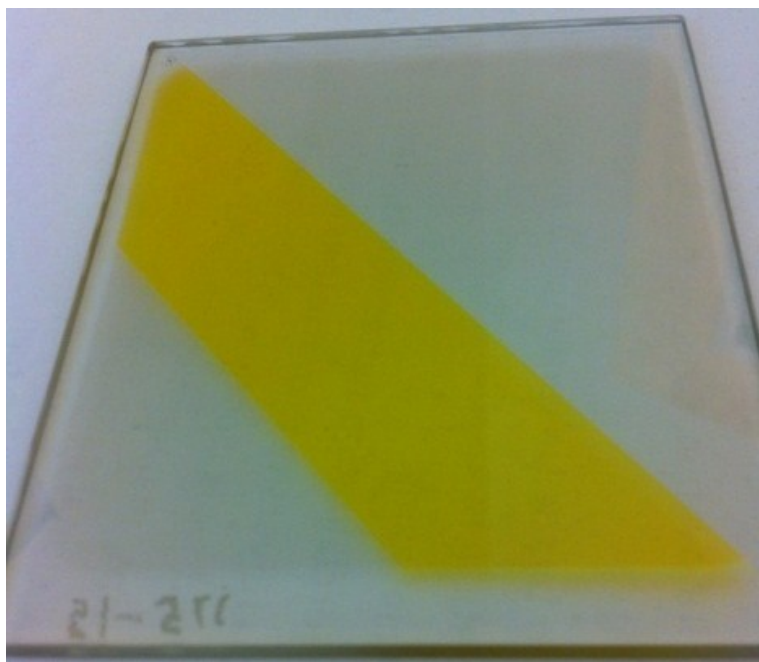


Figure 21. An etched CdS film

There are many methods for evaluating step height values. In the past, these measurements have most commonly been made using a mechanical profilometer. Mechanical profilometers work by dragging a contacting stylus across a surface and analyzing the deflection as the surface is moved relative to the measurement device. High-end profilometers have better than one

nanometer resolutions and can measure steps on the order of several millimeters however there are drawbacks. For one, the stylus can easily damage the surface that it is measuring. Also, since the stylus has a very acute point, its measurements are two-dimensional in nature and can only determine the surface plot of the exact path across which it was drawn. Non-representative characterizations may be made if the stylus is moved over a portion of the surface which contains an anomaly or imperfection.

Rather than using a traditional mechanical profilometer to obtain the step heights across the substrate, scanning white light interferometry (SWLI) was used. SWLI is a non-contacting, optical height measurement made by measuring the interference pattern of coherent beams of white light [38–41]. A white light is beamed at a location on a surface and based off of the reflected light, algorithms are used to quantify the interference pattern and correlate it with a distance measurement. The beam is swept across the surface and a three-dimensional picture is formed of the surface. SWLI is much faster than mechanical profilometry, yet does not sacrifice accuracy. Less than one nanometer vertical resolution can be achieved while scanning volumes as large as 89 x 203 x 203mm.

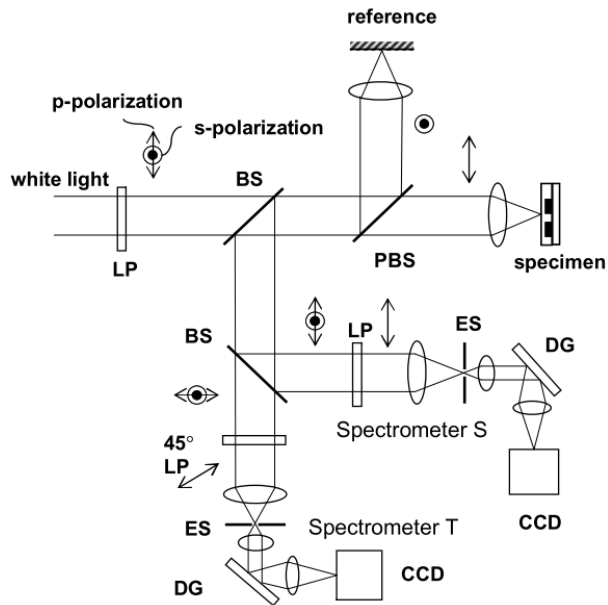


Figure 22. Optical configuration of dispersive white-light interferometry; LP: linear polarizer, BS: beam splitter, PBS: polarizing beam splitter, ES: entrance slit, DG: dispersive grating, CCD: charge coupled device [41]

For this project, a Zygo NewView 7300 3D Optical Surface Profiler was utilized. Fifty, three dimensional pictures were taken of the substrate across the etched diagonal. One such picture, taken at the edge of the substrate, is seen in Figure 23. The software developed by Zygo allows users to analyze these images in many ways. Figure 24 displays how step height data can be derived from the data. A line can be drawn anywhere on the image and displacement measurements are presented as if by a traditional mechanical profilometer. Unlike mechanical profilometers however, the stylus width can be varied to give more representative data if there are imperfections on the surface. From these fifty pictures, fifty step heights were obtained at discrete points to stitch together a complete picture of the representative CdS film thickness across the substrate diagonal.

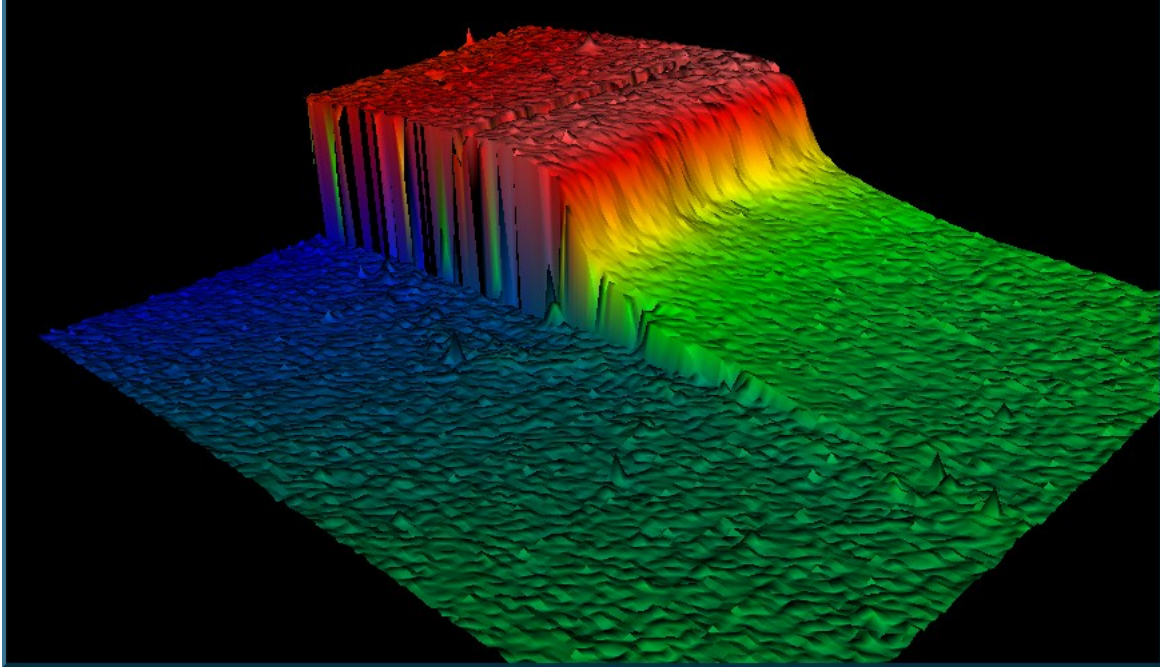


Figure 23. A typical SWLI image

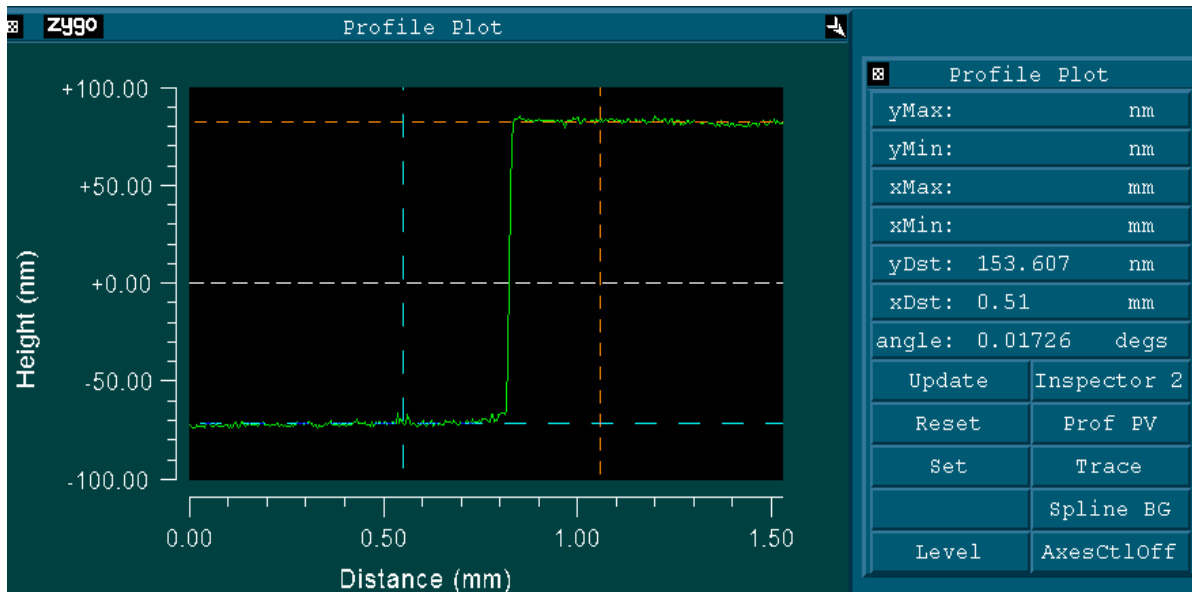


Figure 24. Measurement of the step height from SWLI data

## CHAPTER 3: MODELING CONSIDERATIONS

### 3.1 *Motivation*

Computational Fluid Dynamics is a flow modeling technique that has been used for decades [42], [43]. Aircraft, automobile, boating, as well as numerous industries have invested millions in developing proprietary codes to optimize performance. With an advanced understanding of how differences in geometry and fluid characteristics affect different metrics (lift, drag, thrust, etc.), products and processes can be optimized quickly and easily. Having an accurate knowledge of performance greatly reduces the need for creating and testing prototypes, saving both time and money. Recently, more sophisticated CFD programs have begun to integrate fluid dynamics with multiphase physics as well as chemical reactions to form comprehensive methods for solving most engineering problems.

Though these techniques have been widely utilized in other industries, CFD has to this point, not been widely incorporated into the manufacturing process for thin film photovoltaic panels. Before actual film deposition was modeled, extensive work was performed on modeling the thermal uniformity of the sources. The sources used at the PVMEL were originally designed and analyzed using ANSYS Fluent to predict temperature contours and estimate the amount of thermal shielding required to maintain specific temperatures. This technique was then taken to Abound Solar where it was applied on 2' x 4' deposition sources and shown to be accurate within 2.5% using an IR camera [10].

With the success of the thermal modeling, the decision was made to model the deposition of thin film photovoltaic material using CFD analysis. Chae et. al. had shown promising results with the modeling of thin film deposition for CVD [44], but little to no work to this point has been undertaken to comprehensively model the three dimensional deposition of CdS in CSS.

One of the main reasons that CFD modeling had not been utilized more fully by manufacturers using CSS is that several special considerations need to be taken into account when modeling low pressure flow, heat transfer and chemical reactions simultaneously.

### 3.2 Fluid Mechanics Theory

Within the source, a combination of pressure and convection-driven flows transport Cd and S<sub>2</sub> molecules from the graphite heater to the substrate. In the majority of the flow area, continuum conditions can be assumed and computational solving utilizes the Navier-Stokes equation to characterize flow [45].

$$\rho \frac{Du}{Dt} = -\nabla p + \rho g + \mu \nabla^2 u \quad (3.1)$$

where  $\rho$  is the fluid density,  $u$  is the fluid velocity,  $t$  is time,  $g$  is the gravitational vector, and  $\mu$  is the dynamic viscosity.

However, as most CSS techniques incorporate vapor transport in medium to high vacuum, the standard Navier-Stokes or Fourier momentum and transport equations may not be accurate in all areas [46]. The most accepted way to characterize how strongly these equations will match actual fluid movement is with the Knudsen number, which correlates the average mean free path ( $\lambda$ ) to a characteristic length scale ( $L_c$ ).

$$Kn = \frac{\lambda}{L_c} \quad (3.2)$$

To calculate the mean free path at pressure  $p$ , the following equations were used:

$$\lambda = \frac{k_B T}{\sqrt{2} \pi \sigma^2 p} \quad (3.3)$$

$$\sigma = \sum_{i=1}^{N_g} Y_i \sigma_i \quad (3.4)$$

where  $k_B$  is the Boltzmann constant, equal to  $1.38 \times 10^{-23}$  J/K, and  $\sigma_i$  is the Lennard-Jones characteristic length of species  $i$ . These values were either included in the Fluent material database or were taken from empirical observation [47], [48].

The four Knudsen number regimes are the hydrodynamic, slip flow, transition, and free molecular flow regimes. Fluid flow at atmospheric pressure typically occurs in the hydrodynamic regime where the Knudsen number is less than .01 and particles collide frequently. This flow can be characterized well by normal Navier-Stokes equations. Between Knudsen numbers of .01 and .1, movements are characterized as slip flow and can be described closely by standard equations provided accurate boundary conditions, including temperature jumps and velocity slips at wall-gas interfaces, are provided. As a generally accepted rule, most flows below .05 can use Navier-Stokes without a large diminishment in accuracy. However, in the transition regime, where Knudsen numbers range from .1 to 10, Navier-Stokes and Fourier equations do not define the flow. Either Boltzmann equations or other microscopic models must be used to describe the flow in detail in this regime. Above a Knudsen number of 10, the free molecular flow is governed by particle interactions with the walls much more than with other particles which greatly reduces the accuracy of most models or flow equations [46].

With a Knudsen number of .34 in many areas at normal operating conditions, some of the fluid motion within the source occurs in the transition and slip-flow regimes, in which Boltzmann equations describe the fluid motion more accurately than the Navier-Stokes or Fourier equations. In this pressure range, continuum behavior can be observed away from the source walls but near the walls, a non-negligible “Knudsen layer” is formed [49]. In this

Knudsen layer, molecular collisions with the wall are more dominant than inter-molecular collisions and a no slip assumption is no longer valid. The fluid velocity in the boundary layer at the walls of the cylindrical CdS wells becomes:

$$u(R) = \frac{\alpha_M - 2}{\alpha_M} \lambda \left. \frac{du}{d\hat{r}} \right|_{\hat{r}=R} + 3 \left( \frac{R_g T}{8\pi} \right)^{\frac{1}{2}} \frac{\lambda}{T} \left. \frac{\partial T}{\partial \hat{z}} \right|_{\hat{r}=R} \quad (3.5)$$

where  $\alpha_M$  is some tangential momentum accommodation coefficient based off of particle momentum and surface texture, T is temperature,  $\hat{r}$  is the radial coordinate,  $\hat{z}$  is the axial coordinate, and  $R_g$  is the specific gas constant. The tangential momentum accommodation factor is the ratio of gas molecules that are reflected diffusely to those that are reflected incidentally [50]. These values are difficult to measure but are typically near unity, so Fluent default values were accepted for all species. These low-pressure fluid considerations were enabled in Fluent by turning “low-pressure boundary slip” on.

### 3.3 Heat Transfer Theory

The three basic types of heat transfer are conduction, convection, and radiation. In the deposition process of CdS, all three modes of heat transfer are encountered, however, at the operating pressure used in the ARDS; the effects of convection are negligible compared with that of conduction and radiation.

As with most operations that occur in vacuum, heat transfer in this CSS technique is dominated by radiation heat transfer. Before the substrate is brought over the source, it is radiatively heated by graphite heaters. During the deposition process as well, the substrate is heated by radiation from the top heater and bottom source. Though it is a necessary step, incorporating radiation in CFD modeling greatly increases the computational time required to

solve a given set of equations. Temperatures as well as incident radiation intensities are calculated each iteration for every node on the surface of elements along with each cell within the fluid volume. The basic equation for radiation heat transfer between two black body surfaces is given as [51]:

$$Q_{net} = A_1 F_{1-2} \sigma (T_1^4 - T_2^4) \quad (3.6)$$

where  $A_1$  is the area of surface 1 in  $m^2$ ,  $F_{1-2}$  is the view factor of surface 1 to 2, and  $\sigma$  is the Stefan–Boltzmann constant equal to  $5.670373 \times 10^{-8} \text{ Wm}^{-2}\text{K}^{-4}$ . For this modeling effort, the discrete ordinance (DO) radiation model was utilized, which solves the radiation transfer equation for a finite number of discrete solid angles rather than calculation the view factor from surface to surface. Also in this model, the surfaces are considered gray and are assigned emissivity coefficients according to the material properties. The basic equation for the net radiation flux leaving a surface in a pure vacuum then becomes [52]:

$$q_{out} = (1 - \varepsilon_w) q_{in} + n^2 \varepsilon_w \sigma T_w^4 \quad (3.7)$$

where  $\varepsilon_w$  is the emissivity of the wall and  $n$  is the index of refraction of the material between the wall and another surface.

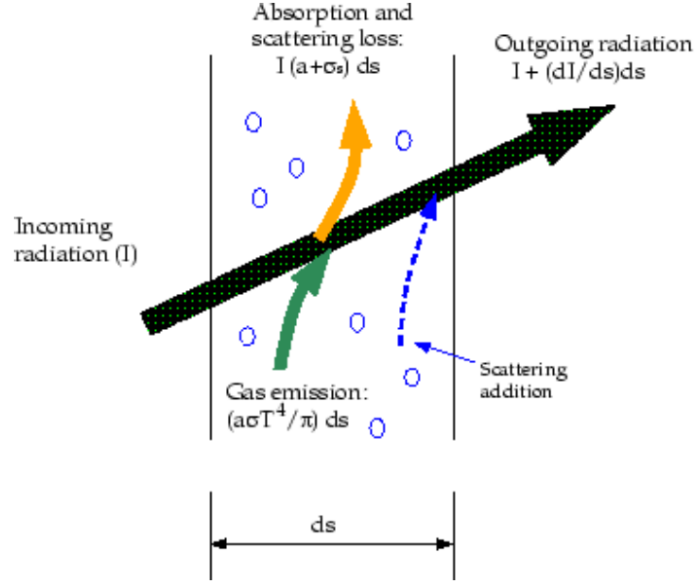


Figure 25. Radiative heat transfer through a fluid volume [52]

The gas within the source also plays a role in how one surface radiates thermal energy to another. Each species absorbs, scatters, and reemits radiation within the fluid volume according to the equation [52]:

$$\begin{aligned} \nabla \cdot (I_\lambda(\vec{r}, \vec{s})\vec{s}) + (\alpha_\lambda + \sigma_s)I_\lambda(\vec{r}, \vec{s}) \\ = \alpha_\lambda n^2 I_{b\lambda} + \frac{\sigma_s}{4\pi} \int_0^{4\pi} I(\vec{r}, \vec{s}')\Phi(\vec{s} \cdot \vec{s}')d\Omega' \end{aligned} \quad (3.8)$$

where  $I_\lambda(\vec{r}, \vec{s})$  is the wavelength dependent radiation intensity on position  $\vec{r}$  in direction  $\vec{s}$ ,  $\sigma_s$  is the scattering coefficient,  $I_{b\lambda}$  is the black body intensity given by the Planck function,  $\Phi$  is the phase function,  $\Omega'$  is the solid angle and  $\alpha_\lambda$  is the absorption coefficient based off of the extinction coefficient  $\kappa$ , and the wavelength  $\lambda$  [53]:

$$\alpha_\lambda = \frac{4\pi\kappa}{\lambda} \quad (3.9)$$

Some of these properties have been empirically evaluated; however, the majority of these values are derived from kinetic theory.

### 3.4 *Chemical Reaction Theory*

The two dominating chemical reactions that occur in the CSS CdS deposition process are the sublimation of CdS from the graphite source and the deposition on the glass substrate. Both of these reactions require different reaction models that take into account the partial pressures of cadmium and sulfur gas, temperature, gas kinetics, and impingement rates.

The sublimation, growth rate reaction, and sublimation reaction for this project were derived from several CdS crystal growth experiments [54–57]. In each of these developed models, a CdS source was held at a higher temperature than a growth section, some distance away. Though these experiments were one-dimensional in nature, many of the assumptions concerning the relationships of Cd and S<sub>2</sub> vapor species hold true in three-dimensional analysis. The two assumptions that governed the development of a surface-wall reaction in Fluent are that the growth and sublimation rates are limited by the transport of species through the vapor phase and that equilibrium is always established between the solid phase and the vapor phase immediately adjacent to it.

At both the source surface as well as the substrate surface, condensation and evaporation reactions are constantly taking place. At the vapor's saturation pressure, the rate of impingement of Cd and S<sub>2</sub> gas molecules on the surface of CdS balances with the rate of these gases coming off the material. If the partial pressure of either species becomes lower than the vapor pressure of that species in the fluid volume directly adjacent to the solid phase, there is a net evaporation. Likewise, if the partial pressure of a species becomes higher than the saturated vapor pressure of the species, a net condensation reaction takes place. Because both of these effects are occurring at both surfaces, re-sublimation from the substrate and CdS growth on the source surface were allowed in the Fluent model.

By making the assumption that CdS dissociates into stoichiometric Cd and S<sub>2</sub>, the equilibrium source pressure,  $P_S^0$ , and the reactions constants,  $K_P$ , can be expressed through the following associations:

$$P_S^0 = P_{Cd} + P_{S_2} \quad (3.10)$$

$$P_{Cd} = 2P_{S_2} = (2K_P)^{1/3} \quad (3.11)$$

$$K_P = P_{Cd}^2 P_{S_2} \quad (3.12)$$

Most of the parameters needed to characterize the growth rate and sublimation reactions were initially calculated by using the Antoine equation for CdS, which correlates the temperature with the partial pressures of Cd and S<sub>2</sub> species in a fluid volume. Though specific values vary from experiment to experiment, this equation can be found by using the empirically derived equation for the reaction constant, fitted to the equation [55], [56]:

$$\log_{10} K_P = \log_{10} P_{Cd}^2 P_{S_2} = -3.45 * 10^4 / T + 20.86 \quad (3.13)$$

with pressure in Torr and temperature in Kelvin. Thus, the general Antoine equation for CdS becomes roughly:

$$P_S^0 = 1.0588 * 10^{10} * e^{\frac{-26141}{T}} \quad (3.14)$$

For all surface-wall reactions, Fluent uses Arrhenius rate equations so the Antoine equations were modified. Coefficients for four Arrhenius rate equations in total were required to describe both processes for both species in the source. The Arrhenius rate equations used in the Fluent code are in the form of:

$$R = A * T^\beta e^{-E_A/RT} \quad (3.15)$$

where A is some pre-exponential factor,  $\beta$  is the temperature exponent,  $E_A$  is the activation energy for the reaction in J/kmol, and R is the universal gas constant in J/kmol-K.

Fluent uses three classifications of materials for use in wall-surface reactions: gas, site, and bulk. The gas classification is simply the species in fluid form. Site refers to the material that is defined as surface-absorbed, meaning that the user defines the quantity and concentration of site material on a given surface. Site species interact with the gas molecules in the adjacent fluid zone. Bulk material is deposited on a surface when a gas molecule is condensed at a site location according to the Arrhenius rate equation and does not react with gas molecules.

The four reactions that required Arrhenius rate equations in the source models are:

1. Cd sublimation:  $S(\text{bulk}) + \text{Cd}(\text{site}) \rightarrow S(\text{site}) + \text{Cd}(\text{gas})$
2. S sublimation:  $2 \text{Cd}(\text{bulk}) + 2 S(\text{site}) \rightarrow 2 \text{Cd}(\text{site}) + S_2(\text{gas})$
3. Cd deposition:  $S(\text{site}) + \text{Cd}(\text{gas}) \rightarrow S(\text{bulk}) + \text{Cd}(\text{site})$
4. S deposition:  $2 \text{Cd}(\text{site}) + S_2(\text{gas}) \rightarrow 2 \text{Cd}(\text{bulk}) + 2 S(\text{site})$

Since the Antoine equations were obtained from one-dimensional experiments, kinetic theory and gas dynamics were incorporated to convert these equations to the correct Arrhenius rate equations used by Fluent. To modify the pre-exponential factor, the molecular impingement rate of an ideal gas hitting a surface was incorporated. The molecular impingement rate,  $\varphi$ , is given by:

$$\varphi = \frac{n\bar{v}}{4} = \frac{\left(\frac{P}{RT}\right)\sqrt{\frac{8RT}{\pi m_i}}}{4} = \frac{P}{\sqrt{2\pi RT m_i}} \quad (3.16)$$

where  $n$  is the molecular density,  $\bar{v}$  is the average molecular velocity, and  $m_i$  is the mass of each species. Pressure is given as a function of temperature in the Antoine equation and by using this, the rate of atoms sublimating from the source surface can be calculated. Because FLUENT uses the specific volume ideal gas constant in their exponential term (8314 J/kgmolK), this needs to be accounted for to get the correct units. With this, equation 3.14 becomes:

$$P_S^0(T) = 1.0588 * 10^{10} * e^{\frac{-2.1734E8}{RT}} \quad (3.17)$$

According to the relationship defined in equations 10 and 11, the partial pressure of Cd is twice that of S<sub>2</sub> because two Cd atoms come off of the surface for every S<sub>2</sub> molecule. Because of this, the saturation pressure from equation 17 must be multiplied by 2/3 for Cd and 1/3 for S<sub>2</sub>.

Fitted to the Arrhenius rate equation used by Fluent, the sublimation reactions are:

$$R_{Cd} = 7.059 * 10^9 * T^{-\frac{1}{2}} * e^{\frac{-2.1734E8}{RT}} \quad (3.18)$$

$$R_{S_2} = 3.529 * 10^9 * T^{-\frac{1}{2}} * e^{\frac{-2.1734E8}{RT}} \quad (3.19)$$

To obtain the Arrhenius rate equations for the deposition of Cd and S, the saturation pressure was replaced with the partial pressure of each species in the fluid volume adjacent to the specified surfaces. Fluent uses molar concentration in mol/m<sup>3</sup>, so the pressure was modified to reflect this. The equations for Cd and S deposition are:

$$\begin{aligned} R_{Cd} &= \frac{P}{\sqrt{2\pi RTm_i}} = \frac{[Cd(g)] \times RT}{\sqrt{2\pi RTm_i}} \\ &= 3.431 \times T^{1/2} \times [Cd(g)] \end{aligned} \quad (3.20)$$

$$R_{S_2} = 4.542 * T^{\frac{1}{2}} * [S_2(g)] \quad (3.21)$$

A “sticking coefficient” was used to modify the pre-exponential factor in the Arrhenius rate equation for the deposition reactions. It is the ratio of impinging molecules that contribute to the crystal growth to the number of molecules that are reflected back into the fluid area. It was determined after initial modeling was completed and compared to the experimental results. For all experimental sets tested, it was found that the sticking coefficient was around 0.143.

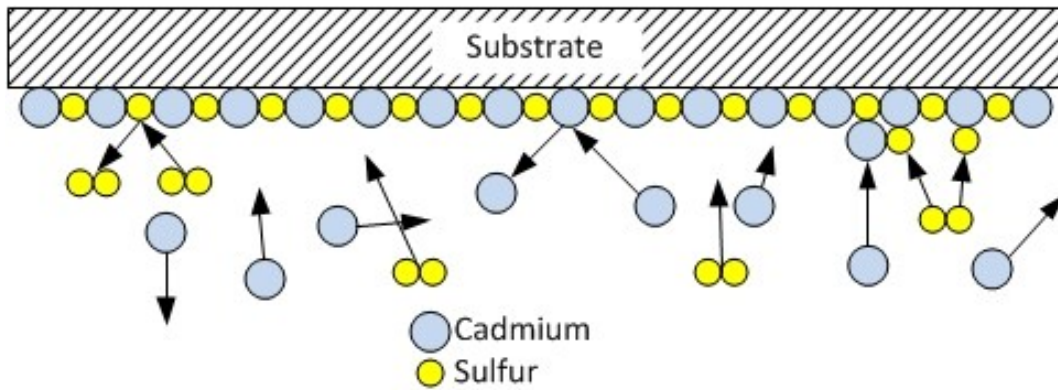


Figure 26. Molecular motion in the fluid volume of the pocket

### 3.5 Computational Resources

At the PVMEL, two servers are dedicated to running full time CFD calculations. Each server is capable of utilizing 192 GB of RAM across 24 cores and every processor operates between 3.46-3.47 GHz. For larger analysis, such as for the complex 3D thermal and fluid model, both servers can be linked together to more quickly run calculations across the 48 cores. During these large calculations, the servers typically exhaust all CPU and between 200-300 GB of RAM. Even with all of this computational power, running the largest of these analyses required over a week worth of nonstop calculations.

## CHAPTER 4: CHEMICAL REACTION RATE MODEL

To make an initial fluid model of the CdS deposition source, the fluid volume within the source was discretized into 150,840 hexahedral and wedge-type cells. The sublimation and growth reactions were modeled using the developed Arrhenius rate equations which were applied to the source and substrate surfaces. Also, the discrete ordinates radiation option was enabled which included the effects of thermal radiation from surface to surface as well as through the fluid volume. The resulting model contained relatively few cells, all with acceptable quality, to ensure that the model was accurate and converged as quickly as possible. From this iteration of modeling, realistic pressure gradients, temperature gradients, species diffusion, fluid velocities, and deposition rates could be measured.

Many assumptions were still made in this model, which could not be corrected until later thermal and fluid models were created. Most notably, the temperature at the walls and the substrate were assumed to be constant throughout the entire deposition process. The source walls, including the wells, pocket walls and area of sublimation were held at 883.15K, while the substrate and the end effector were held at a constant 693.15K. This assumption created non-ideal thermal gradients, but this was assumed to not affect accuracy to a large amount. Another assumption that was made was that the fluid within the pocket is initially all nitrogen. In reality, the operating gas within the ARDS is 98% nitrogen and 2% oxygen. In reality, there exists a reaction between the Cd gas and O<sub>2</sub> molecules, but for the scope of this project, it was deemed too difficult to experimentally measure and not enough information could be found on the subject to effectively include it in the model.

In Figure 27, the molar fraction of Cd gas in the middle cross section of the source can clearly be seen. Similar to the two-dimensional chemical reaction rate source, both cadmium and

sulfur diffuse nearly ideally in the pocket. The species concentrations are highest near the source and lowest near the substrate. It was observed that the species diffuse largely as a function of proximity to the source as well as a function of pocket geometry.

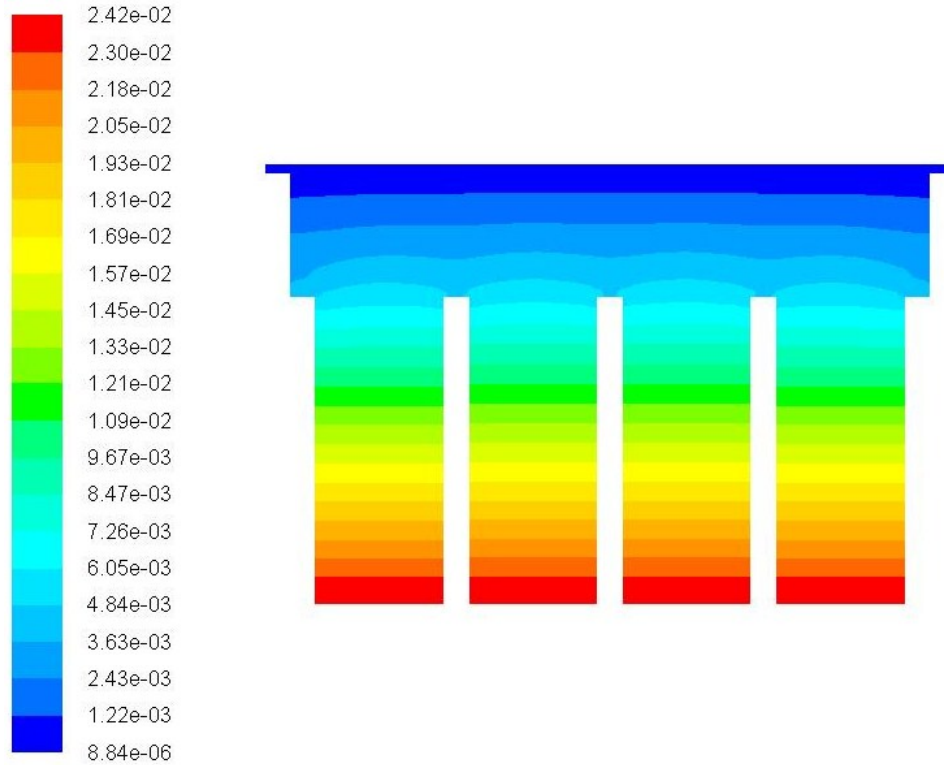


Figure 27. 3D chemical rate model: Cd molar fraction in the source

Possibly the most desired result that was obtained through this modeling was the theoretical CdS deposition rates on the substrate. Figure 28 depicts the substrate overlaid with the local deposition contours of bulk Cd for the given modeling scenario, with each line indicating a 1% change in deposition rate. However, as CdS growth rate is not a recognized metric in Fluent, the deposition rate of bulk Cd was used to calculate the simulated deposition rate of CdS according to the equation:

$$G_{cds} = \frac{R_{cd}}{\rho_{cds} * St_{cds}} \quad (4.1)$$

where  $G_{CdS}$  is the growth rate of CdS in nm/s,  $R_{Cd}$  is the deposition rate of solid Cd in  $\text{kg/m}^2\text{-s}$  calculated from the Arrhenius rate equation specified in Fluent,  $St_{CdS}$  is the mass fraction of Cd in stoichiometric CdS, and  $\rho_{CdS}$  is the density of CdS in  $\text{kg/m}^3$ . Experiments have shown that the deposition rate for most thin films is linear over time for a given source and substrate temperature [35], [36], [54], [56], [58–61], so the derived deposition rate of CdS was simply multiplied by the deposition time to estimate the thickness of the film for a given condition.

From the species calculations, the deposition rates of CdS on the substrate could be analyzed. After applying the sticking coefficient, these results were nearly identical to the CdS thickness values observed experimentally (Figure 45). The sticking coefficient that was calculated in the modeling was 0.143. This means that theoretically, about one in seven molecules that impinges upon the substrate contributes to the growth of CdS crystals. Whether this value is realistic or reflects some calculation error within the Arrhenius rate equations has yet to be experimentally determined.

With the accuracy of the model, an experiment was proposed to use this modeling technique to predict the deposition of a source that had yet to be evaluated. This experiment is expounded upon more fully in Chapter 5.

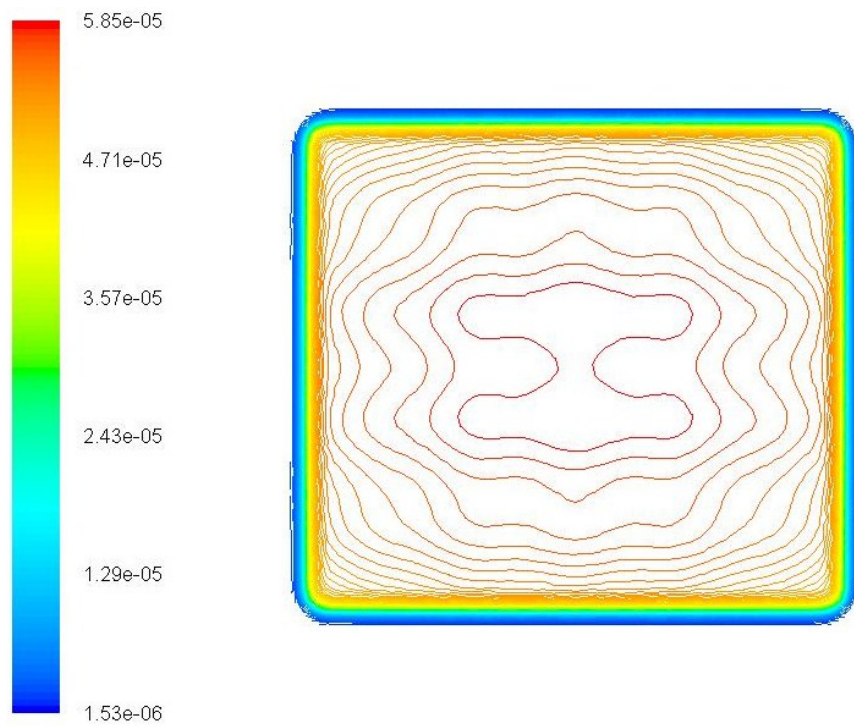


Figure 28. 3D chemical rate model: Deposition rate of Cd on the substrate (kg/m<sup>2</sup>-s)

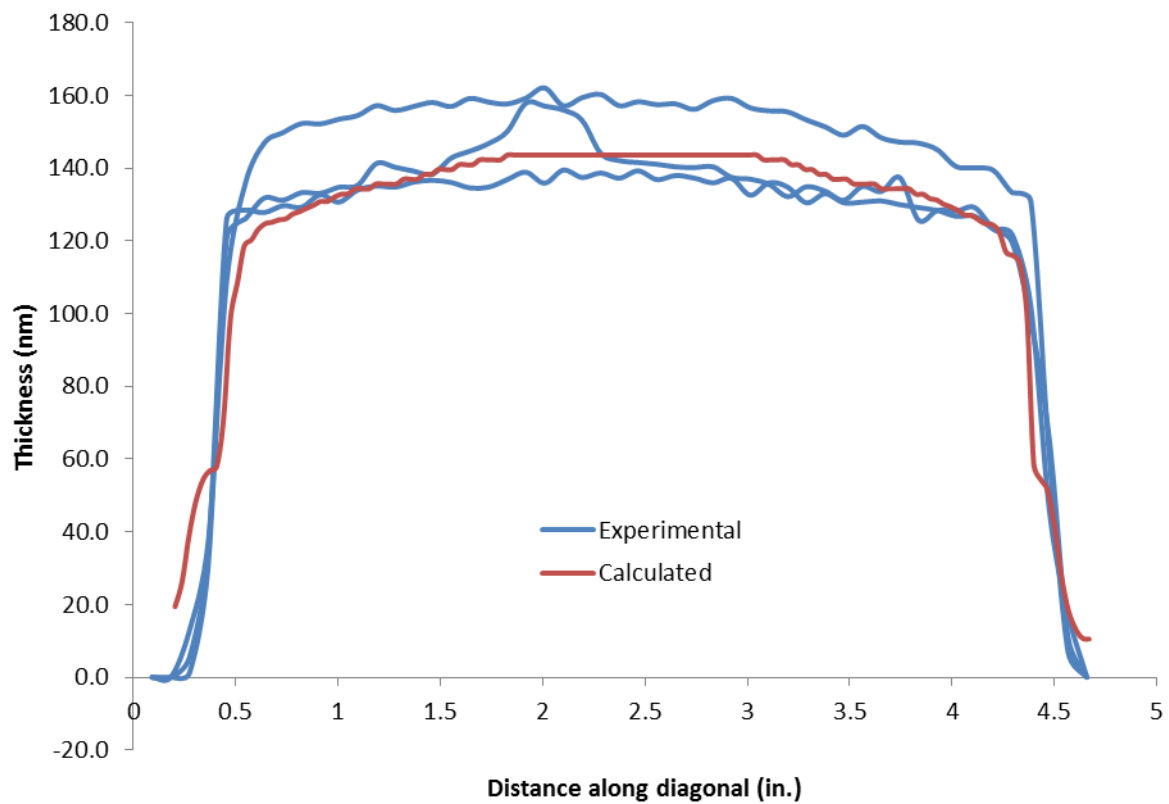


Figure 29. Film thickness across the substrate: Chemical reaction rate source

The temperature gradient, displayed in Figure 30, is strongly tied to the temperature of the local walls. The temperature gradients are not fully comprehensive due to the specification of a constant temperature of the walls over time. Including transient thermal analysis of the source as well as the radiation shielding in the ARDS is needed to completely and accurately temperature profiles.

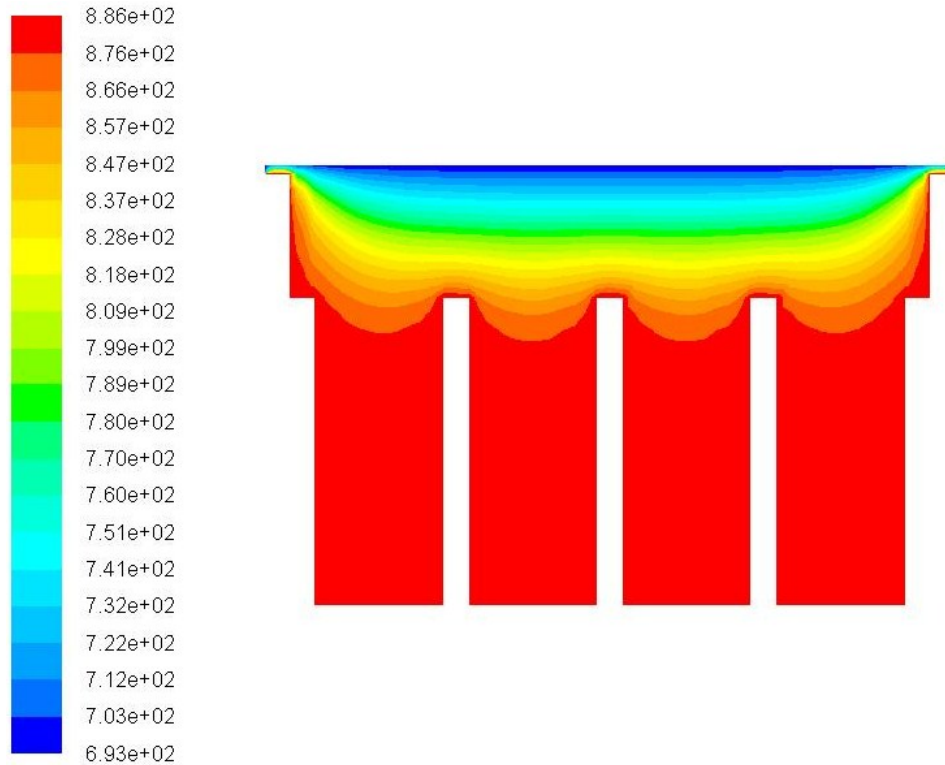


Figure 30. 3D chemical rate model: Temperature in the pocket (K)

This model included the effects of thermal radiation in the pocket for the first time. The amounts of incident radiation are highly dependent on both the geometric coordinate relationships of each node and the temperature of each surface. One of the reasons that the sources were designed in the manner that they were is so that the sublimating photovoltaic material does not have a large view factor of the much colder substrate. It was thought that if the sublimating material had too large of a view factor of the substrate, the material would cool

below sublimation temperatures and no deposition would occur. In Chapter 6, this assumption was experimentally proven to be false.

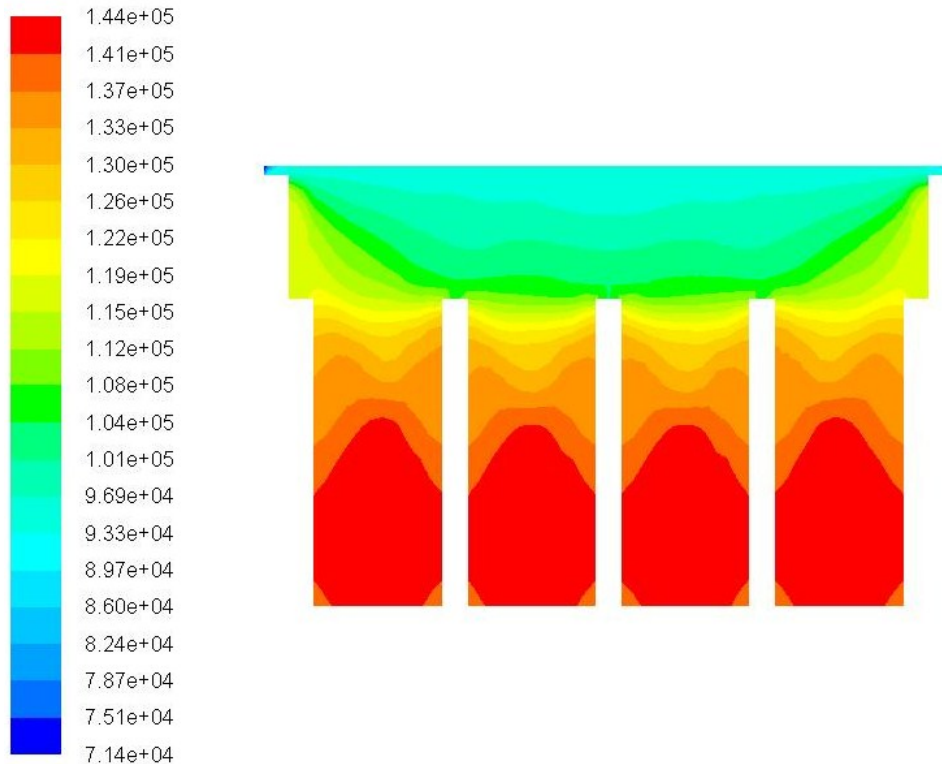


Figure 31. 3D chemical rate model: Incident radiation in the pocket ( $\text{w/m}^2$ )

In the source that is typically used for deposition, heat transfer within the pocket is dominated by radiation. With radiation heat transfer enabled, the CdS source surface was seen to lose around 3.69 Watts due to radiation, while the radiative heat flux on the substrate surface was 116.85 Watts. With radiation heat transfer disabled in modeling, the surface of the CdS source lost less than 0.2W of heat, and the heat flux of the substrate was only 5.2Watts. From this, it can be observed that radiation is the dominant form of heat transfer within the pocket, accounting for 95% of the heat transfer on the source and 96% of heat transfer on the substrate.

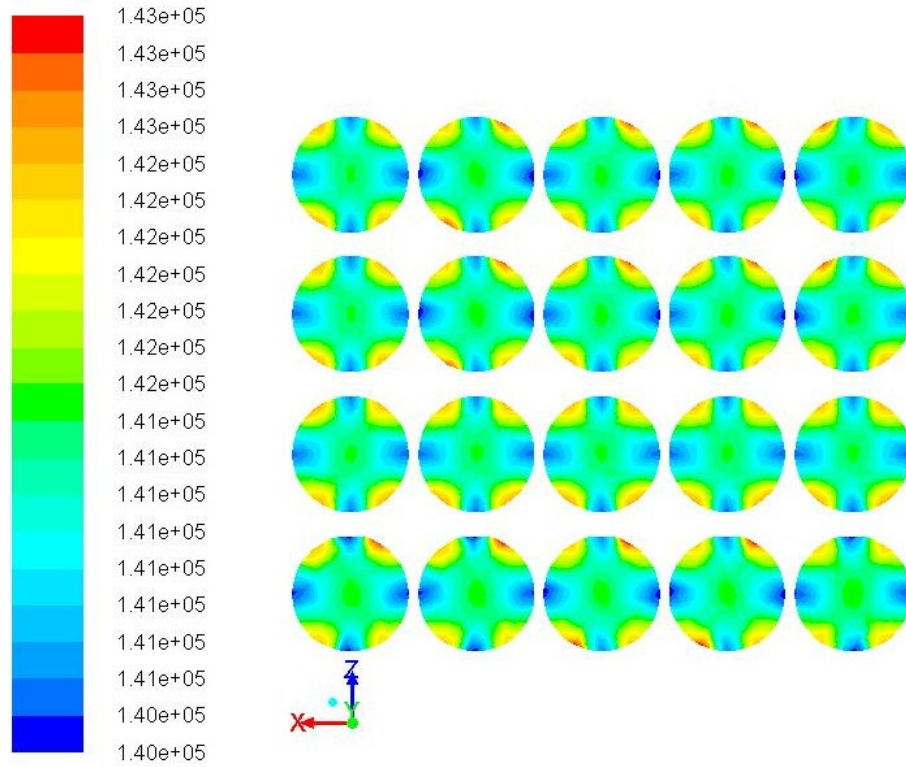


Figure 32. 3D chemical rate model: Incident radiation on the CdS source surface (w/m<sup>2</sup>)

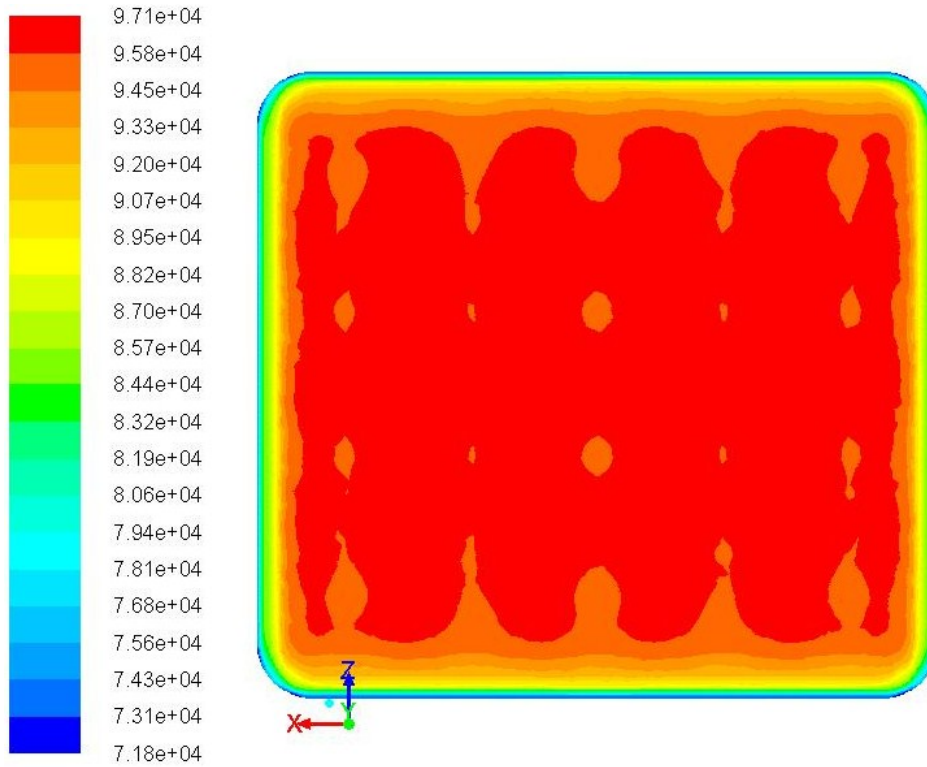


Figure 33. 3D chemical rate model: Incident radiation on the substrate (w/m<sup>2</sup>)

## CHAPTER 5: PREDICTING FILM GROWTH IN AN ALTERNATIVE SOURCE

### 5.1 *Motivation*

The motivation behind the entire modeling effort at CSU is to model the deposition of thin film photovoltaics in the sources used in the ARDS using CFD applications and ensure that the models can be used to predict material growth in sources that have not yet been built, with increasing film uniformity on an industrial scale in view. A large transitional step in this process is to create a modified new source and validate the accuracy of the model by comparing the predicted results with the actual results. If the calculated results from the altered model closely matched the experimental results there would at least be proof of concept for using CFD analysis to predict CdS growth before manufacturing a source.

Further motivation for creating a more uniform source came from the manner in which the solar cells from the ARDS are tested. Researchers use each 3" x 3" solar cell to create nine small area devices (SADs) from which, properties such as short circuit voltage, current density, and efficiency are calculated. SADs are created in the PVMEL by taking a completed solar cell from the ARDS, masking nine, equally spaced, quarter-inch circles on the film, and removing everything except the TCO. A metallic back contact is added to the nine circles and the entire cell is placed on a light box to test the electrical properties. Ideally, all nine SADs would have identical properties, but in reality, properties vary from SAD to SAD. Much of this variation is linked to the non-uniform film deposition, along with non-uniform CdCl<sub>2</sub> and heat treatments.

### 5.2 *Description of the Modified Source*

The previous design of the sources used in the ARDS did not use computer modeling or take into account the complex fluid mechanics within the source. Rather, the assumption was made that molecules from the source travel linearly to the substrate and that the most important factor

in the sublimation reaction is the view factor of the colder substrate from the photovoltaic material. Applying computational methods and experimental validation however, has shown that many factors affect the deposition and that the fluid moves according to the Navier-Stokes as well as Boltzmann equations for low pressure flow. With enhanced understanding of the background physics, researchers could predict which source parameters affect film uniformity. It was decided that in a new deposition source, the pocket dimension should be increased, while the well dimension should be decreased to increase uniformity. As the deposition of CdS had shown to be diffusion limited in the 40mTorr range (Figure 15), increasing the volume that the vapor has to diffuse was thought to lead to a more uniform film deposition.

Instead of designing, manufacturing, and testing a completely new source, the decision was made to utilize a previously created PECSS source. The PECSS source uses the same method of embedded heaters to increase the temperature in a graphite source until a photovoltaic material sublimates as the normal source. However, as this source is typically used to create a plasma within the pocket, the pocket depth is much greater than the normal source. The pocket of the PECSS source is 1.5" deep, 1" deeper than the normal source, and the wells are .375" deep, 7/8" shallower than the normal source. For this experiment, the anode wire and gas injection ports were closed and the deposition process became solely CSS.

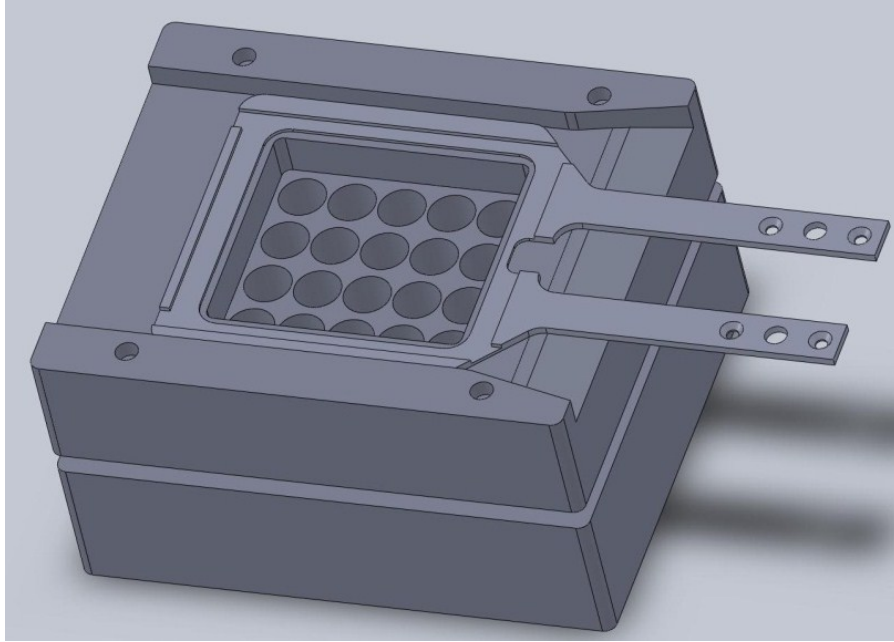


Figure 34. Normal graphite source geometry: With end effector

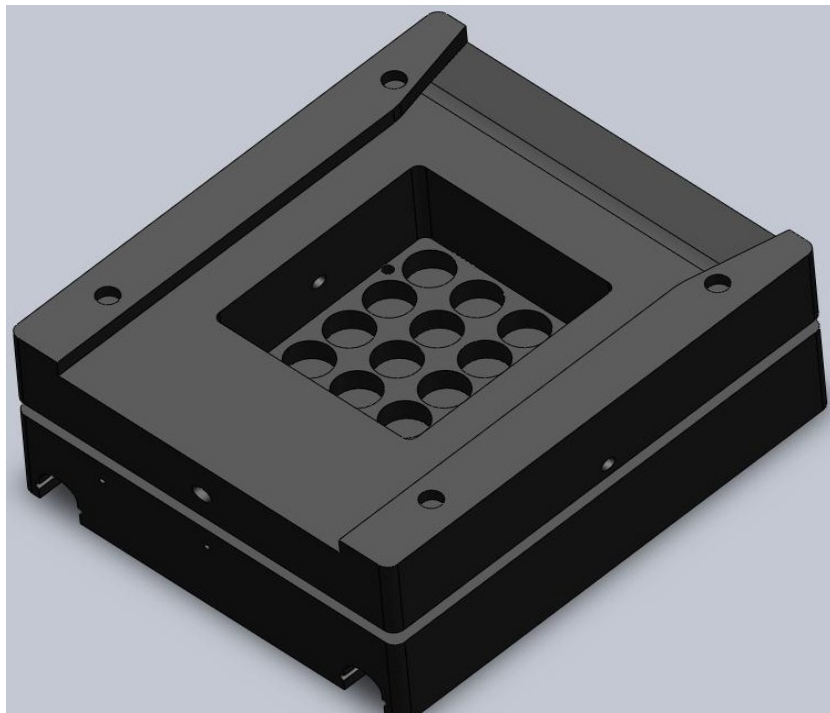


Figure 35. Modified source geometry

The model for this source was developed much in the same way that the model for the three-dimensional chemical reaction rate source was developed. A mesh was created to ensure

enhanced accuracy in the volume near the substrate. The mesh consisted of 175,428 hexahedral and wedge-type cells with a maximum skewness value of 0.861. Similar to the three-dimensional chemical reaction rate source model, the modified source model used only Arrhenius rate equations specified at the sublimation and substrate surfaces to govern both reactions. The source walls were kept at a constant 883.15K, while the substrate surface was held at 693.15K

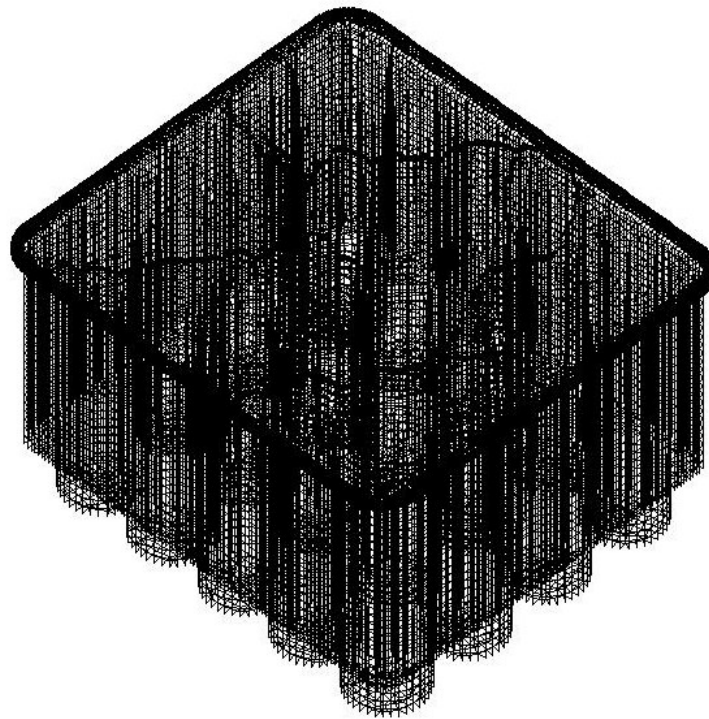


Figure 36. Modified source mesh

### 5.3 Results

From the modeling, it was immediately apparent that the modified source would theoretically lead to more uniform film deposition. In Figure 37, the calculated contours of Cd deposition are displayed, where each line corresponds to a 1% change in film thickness. From the figure, it can be observed that the change in thickness should be slightly less than 1% from corner SAD to

corner SAD. This would be a large improvement from the current method of deposition in which the variation from these locations is around 3% (Figure 38).

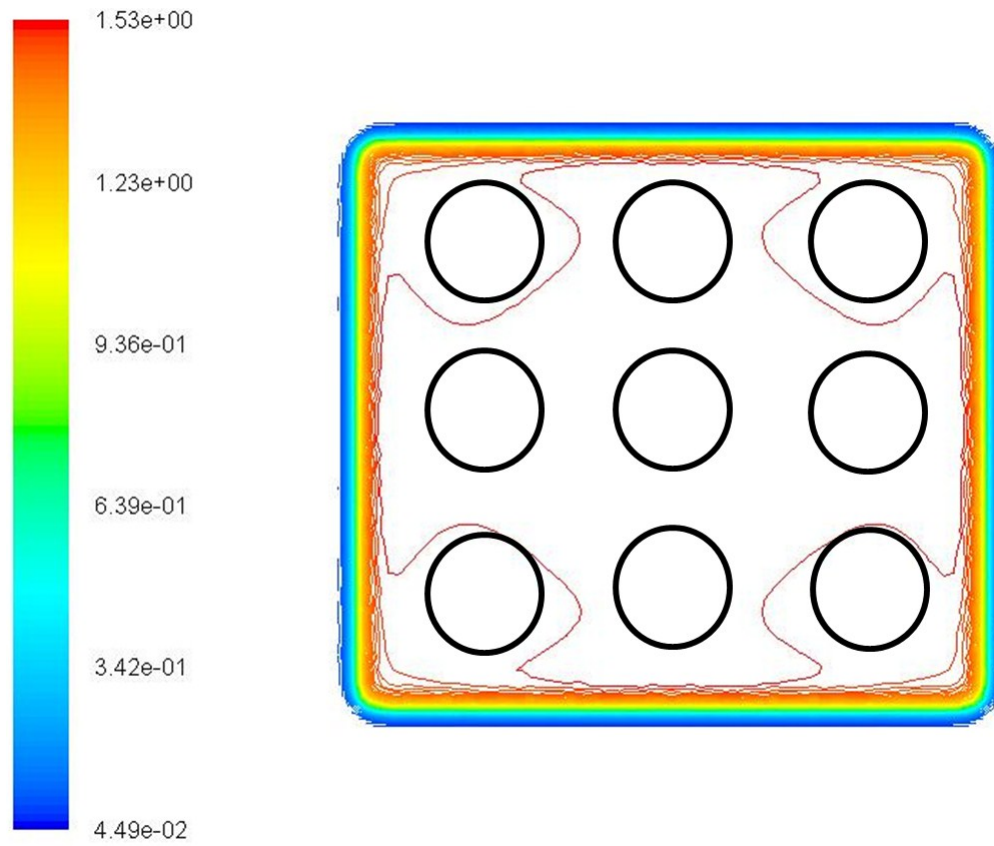


Figure 37. Modified source model: Local CdS deposition rates overlaid with approximate SAD locations on the substrate

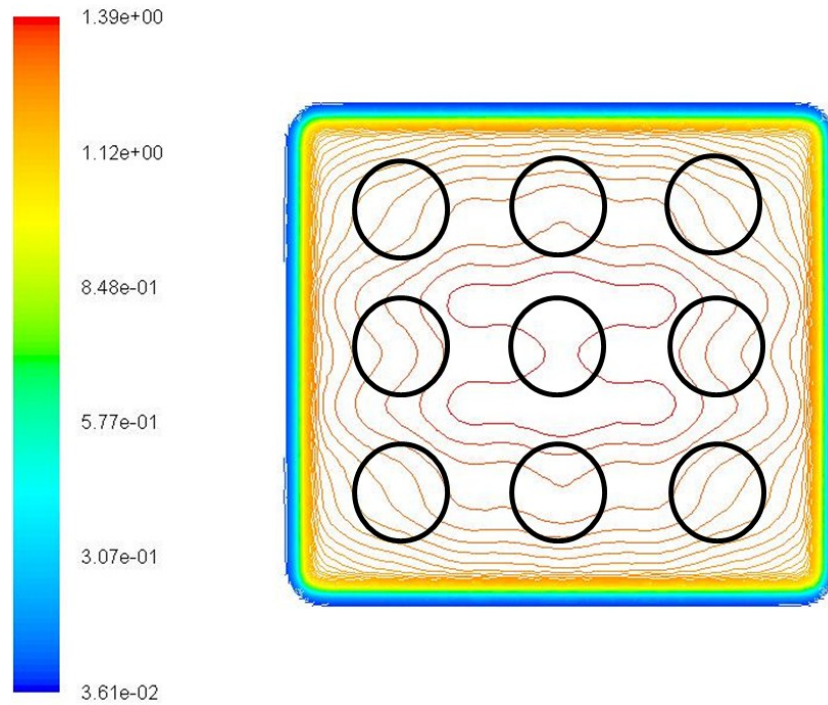


Figure 38. 3D chemical reaction rate model: Local CdS deposition rates overlaid with approximate SAD locations on the substrate

To understand why the modified source led to more uniform deposition, the pathlines for each source were plotted and evaluated. From the normal source, it can be observed that the fluid moves through the wells smoothly then diffuses somewhat before hitting the substrate. By comparison, the modified source allows for much more diffusion by having a much deeper pocket. This result makes sense intuitively, and contradicts the initial presuppositions that were made when the source was first designed, that having a longer well with a small substrate view factor is optimal source design.

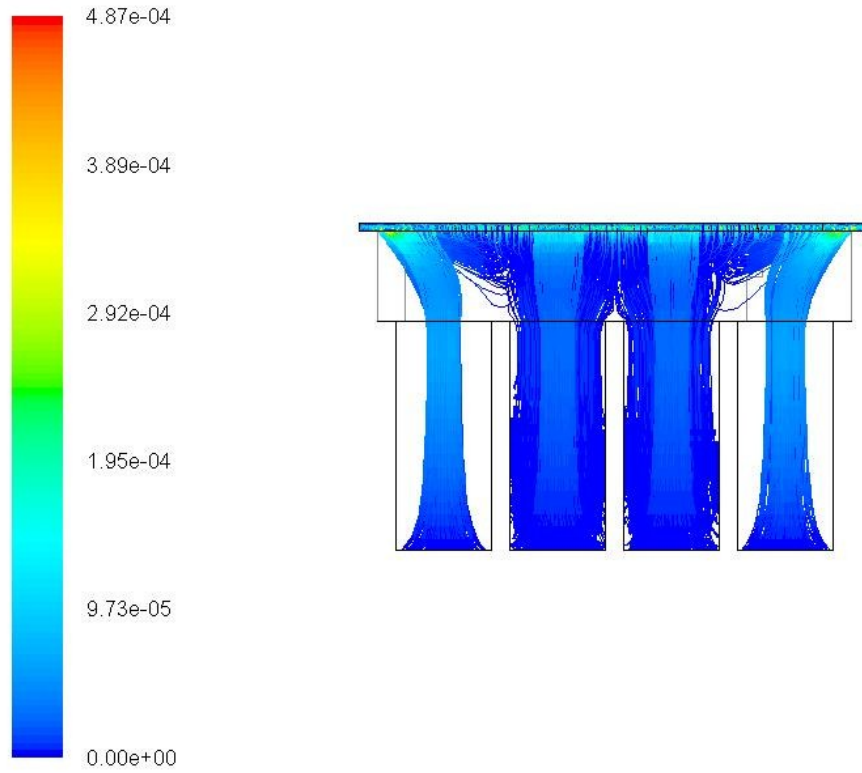


Figure 39. Normal source: Pathlines colored by velocity magnitude (m/s)

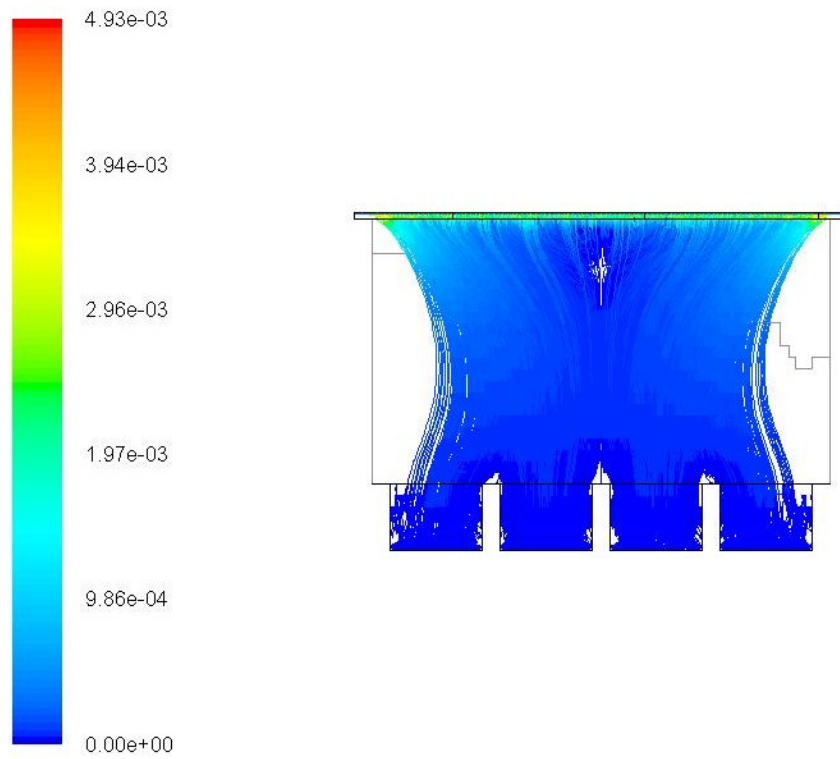


Figure 40. Modified source: Pathlines colored by velocity magnitude (m/s)

The contour plots of species diffusion within the pocket were used to understand why the modified source led to more uniform film growth. By comparing Figure 41 and Figure 42, it can clearly be seen that the molar fraction of Cd gas is more uniform as it reaches the substrate surface compared to the source typically used for deposition. This makes sense intuitively as the pocket of the modified source is much larger and allows for the gas to diffuse more evenly before it reaches the substrate. As noted in section 2.1, the rate of CdS deposition is diffusion-limited, so it assumed that the gas follow's Fick's law for diffusion[62]:

$$J = -D\nabla\varphi \tag{5.1}$$

where J is the diffusion flux rate, D is the diffusion coefficient, and  $\varphi$  is the species concentration. The larger the volume that the gas is allowed to diffuse through, the smaller the species concentration gradient will be.

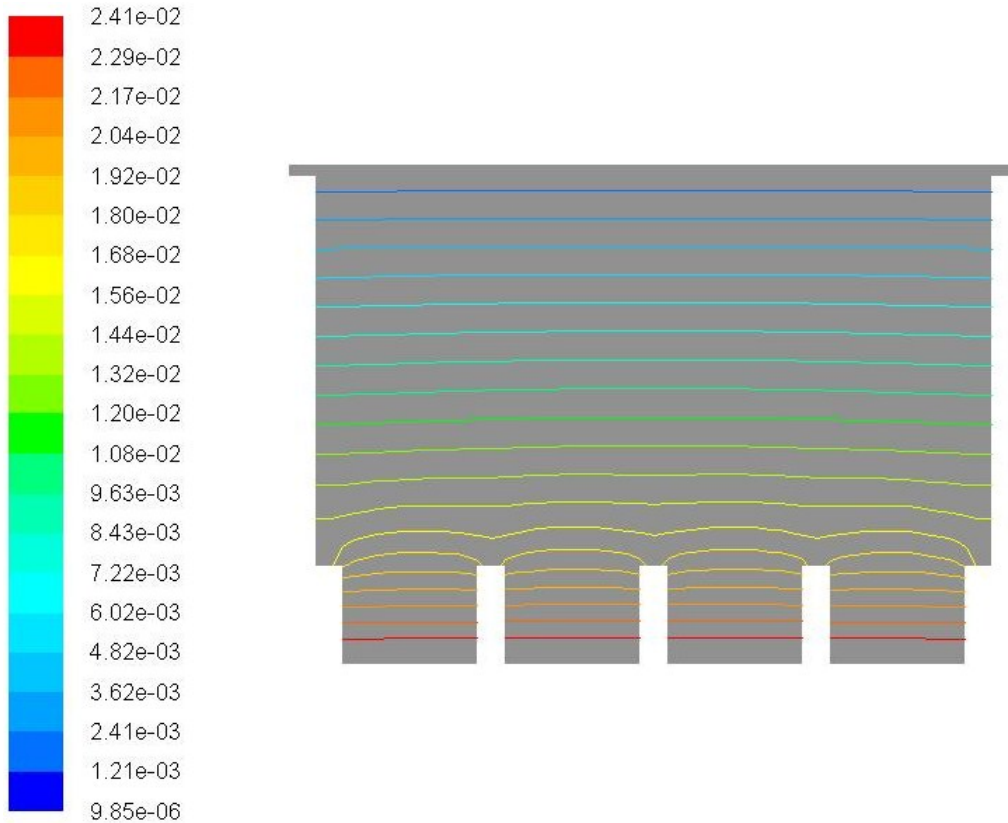


Figure 41. Modified source: Cd molar fraction in the source

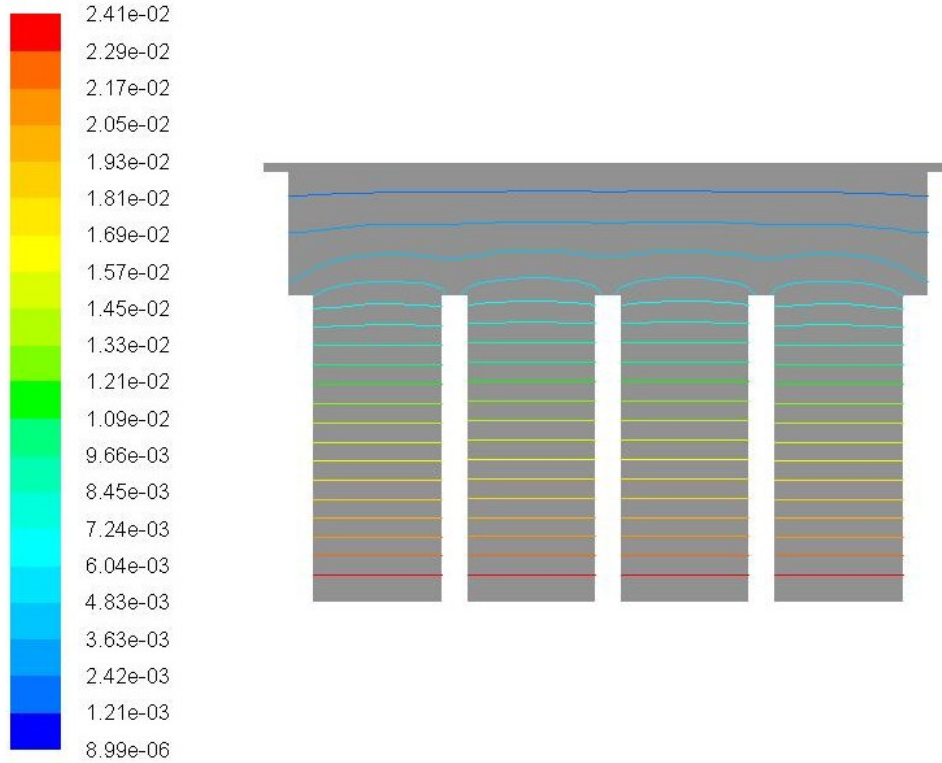


Figure 42. Normal source: Cd molar fraction in the source

The view factor for each well in the modified source is 0.480. This much larger than the view factor of the wells in the normal source, which is 0.123. After calculating the heat fluxes, it was again observed that radiation is the dominant method of heat transfer within the pocket however, when experimentally creating these sample cells, the larger view factor did not result in the rapid cooling of the sublimation surface, stopping the reaction, but rather led to more uniform film deposition. In the modified source, the calculated radiation heat flux on the CdS source was 6.63Watts and accounted for 96% of the total heat transfer on the surface. Likewise, the radiation heat transfer rate on the substrate was 114.95Watts, responsible for 96% of the total heat flux. Though the radiation heat transfer rate is higher in the modified source, experimental results showed little effect on the deposition rate of CdS.

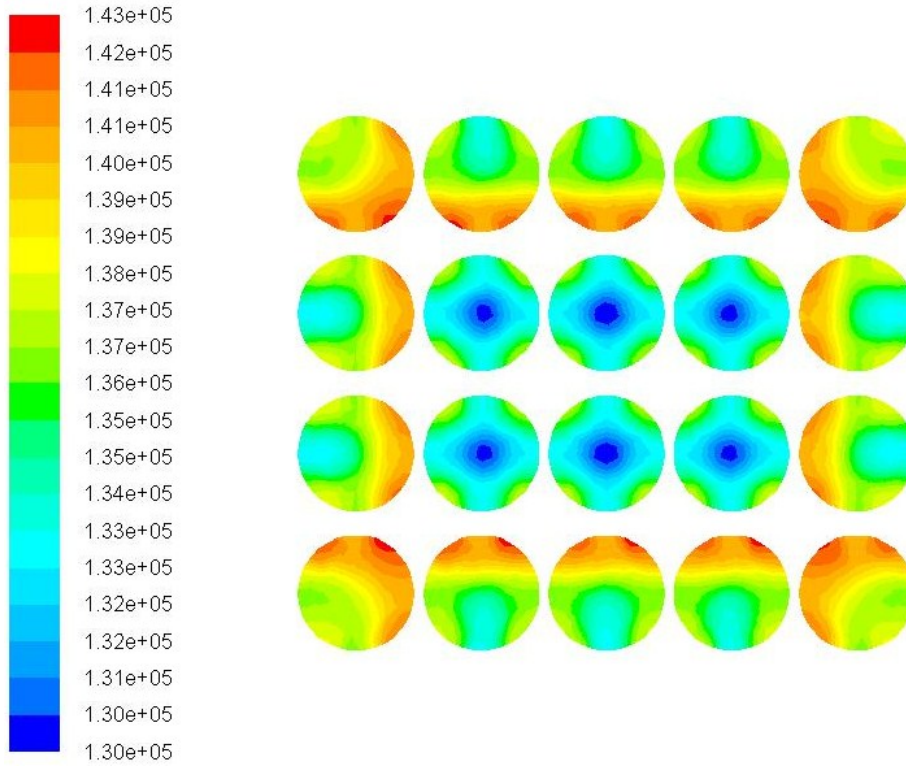


Figure 43. Modified source: Incident radiation on the CdS source surface ( $\text{w/m}^2$ )

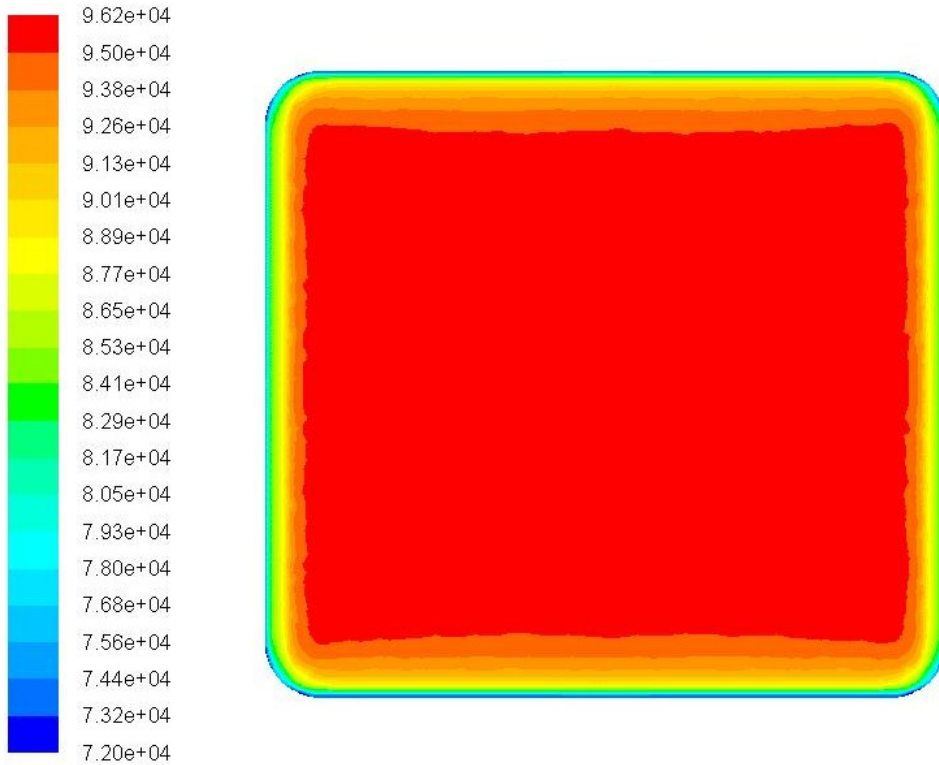


Figure 44. Modified source: Incident radiation on the CdS source surface ( $\text{w/m}^2$ )

To experimentally validate these results, three CdS films were created using the normal deposition source, and three CdS films were created using the modified PECSS source. All substrates were created in a single run, one after the other. This was done to ensure that there were no outside factors affecting the deposition and so that the results could be compared with the previously validated findings from the normal source model and experimental data (Figure 29). The same experimental technique was followed for all six films of masking and etching the films, then using SWLI to measure the step heights at 50 discrete locations.

After creating the CdS films and evaluating the step heights using SWLI, the data was plotted next to the calculated results from Fluent. Figure 45 shows that the model nearly perfectly described the actual film thickness contours across the substrate diagonal with the same sticking coefficient applied. With enhanced resolution in the modeling and in the data collection, it may be possible to further evaluate the accuracy of the model. However, the accuracy of this preliminary model demonstrates at least proof of concept that CFD modeling can successfully be used to predict CdS deposition in sources that have not yet been manufactured or tested.

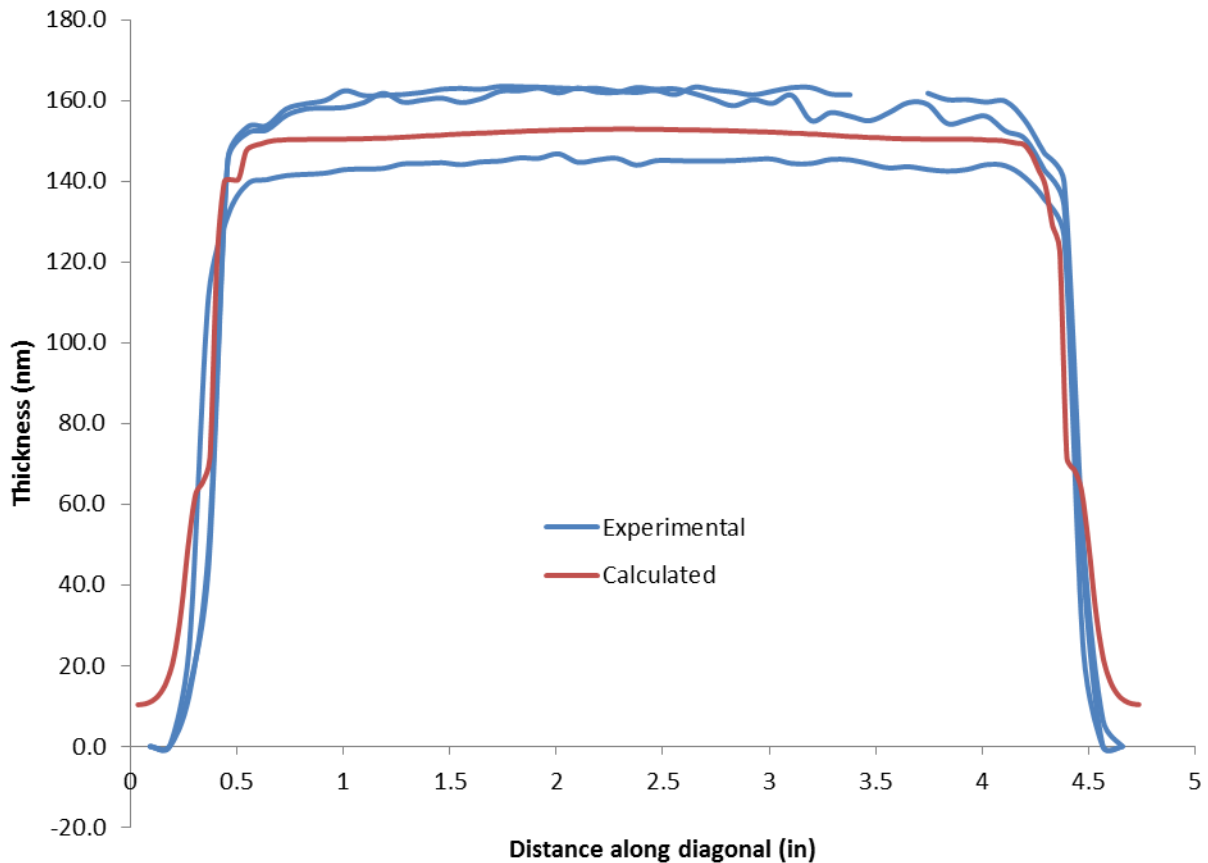


Figure 45. Film thickness across the substrate: Modified source

Also of great importance, the enhanced understanding gained from modeling allowed for the formulation and testing of a source that improved the uniformity of the deposited CdS film layer. The experimental data gathered from the two sources was used to quantify the improvement in film uniformity. The film thickness values between the areas where the corner SADs are made were taken, and the normalized standard deviation between these two locations on the substrate was calculated and averaged for each source. For the normal source, the normalized standard deviation in this region was 2.89%, which means that the thickness varied on average nearly 3% between SADs. The films created by the modified PECSS source varied only 0.83% in this same region. By making a simple source geometry change, and utilizing knowledge of fluid mechanics, the uniformity in the most important area of the substrate was increased by 71.16%.

These results were groundbreaking and have since led to substantial reductions in the variation of electrical properties from SAD to SAD.

## CHAPTER 6: DISCUSSION AND FUTURE WORK

### *6.1 Discussion of Results*

An accurate CdS growth rate model was created by incorporating fluid mechanics, heat transfer, and chemical theory into a comprehensive CFD model. The model closely predicted the actual deposition values both quantitatively and qualitatively. In combination with the validated source thermal modeling that has been used to optimize source geometry and operating processes, it may be surmised that CFD analysis is useful and prudent for the design and optimization of CSS sources for thin film applications.

### *6.2 Combined Thermal and Fluid Modeling*

The next step in enhancing the accuracy of the model is to combine the experimentally validated fluid model with a transient thermal model. This will ensure that the sublimation reaction is correctly depicting a sublimation event and not simply specifying a flux rate for a given model. Linking the fluid and thermal models together also guarantees that more realistic thermal gradients and transient thermal effects would be taken into account. The temperature along the source wall is not constant in reality, but rather varies with proximity to the embedded NiCr heating elements, the amount of local thermal radiation, and time.

An initial two dimensional and simple three-dimensional thermal and fluid models have been created to provide proof of concept for the sublimation reaction and incorporation of transient thermal effects. Basic assumptions were made that decreased computational time but also decreased the accuracy of the models to the extent that any results could not be considered representative.

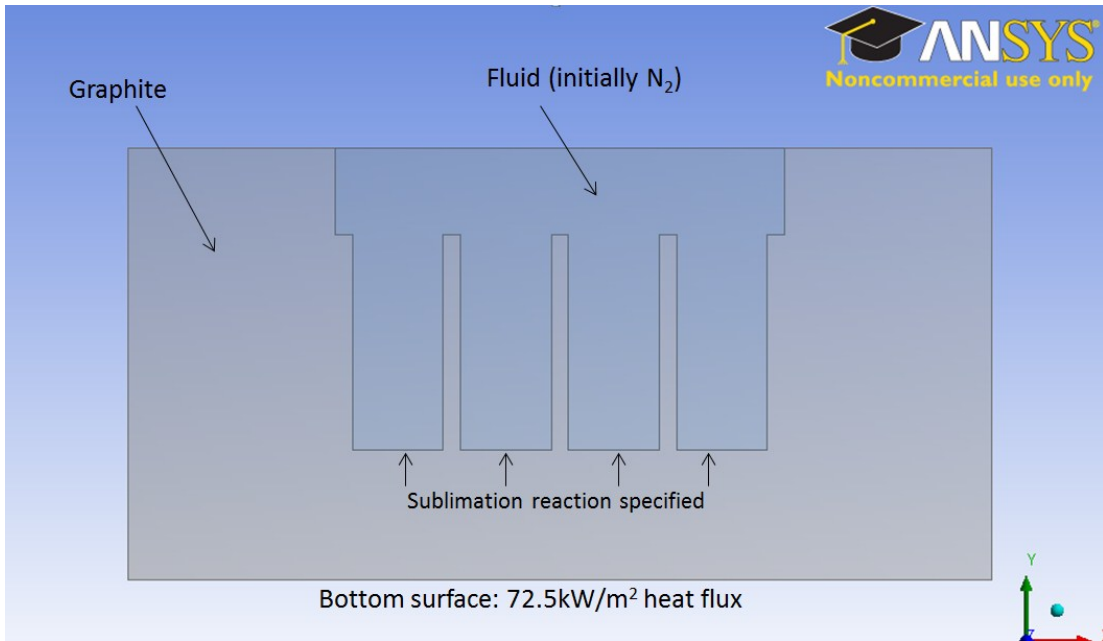


Figure 46. 2D thermal and fluid model: Geometry

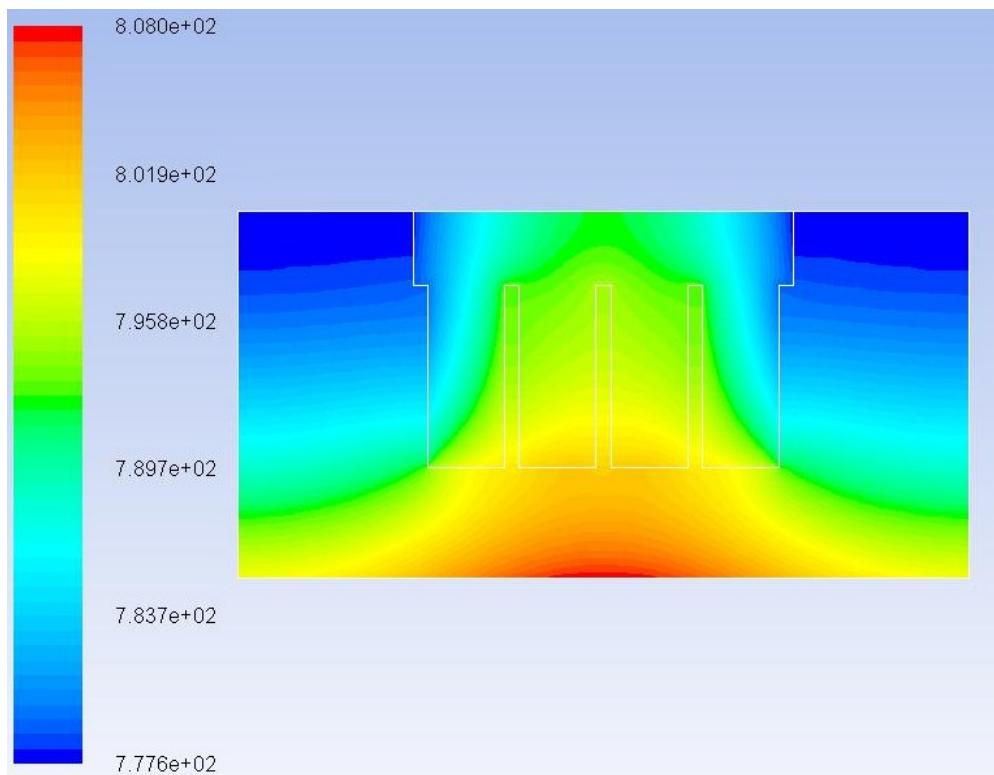


Figure 47. 2D thermal and fluid model: Temperature in the source (K)

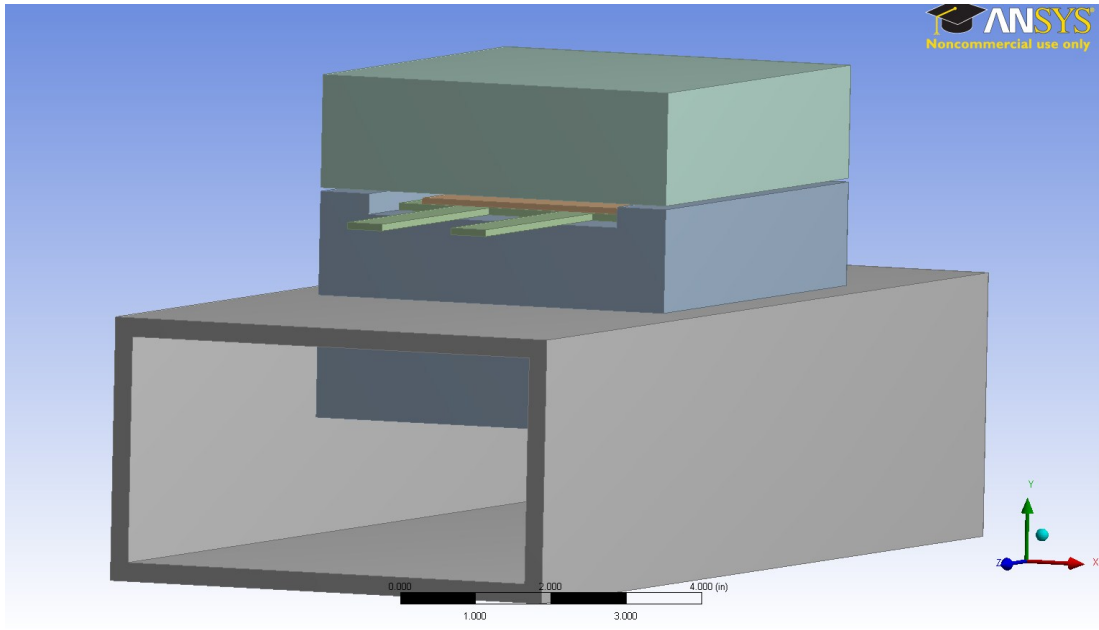


Figure 48. Simple 3D thermal and fluid model: Geometry

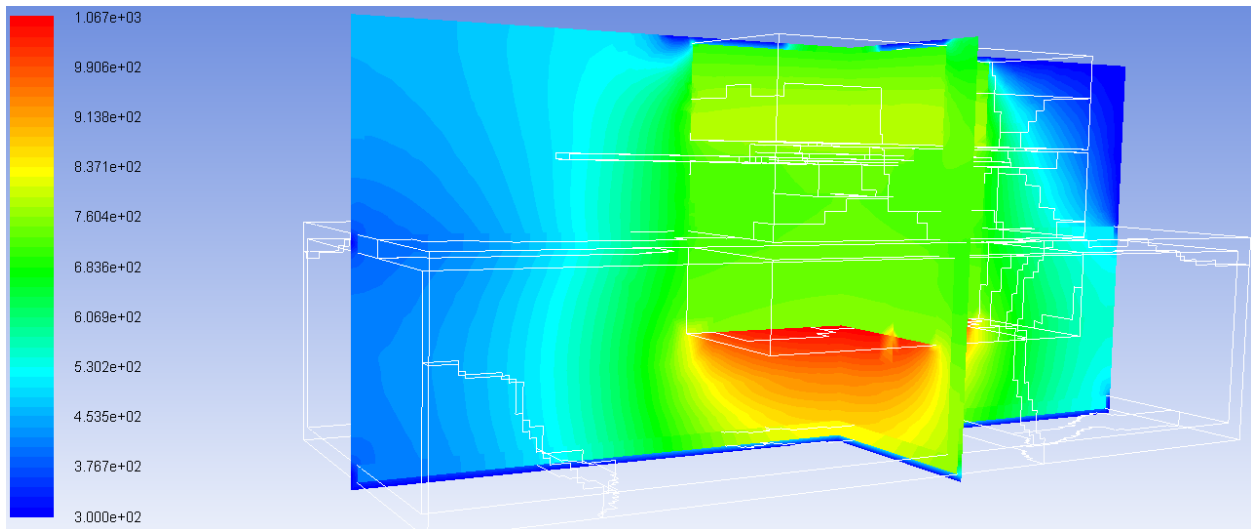


Figure 49. Simple 3D thermal and fluid model: Temperature in the source (K)

The final step in modeling the sublimation and deposition of CdS in CSS is to create a fully comprehensive source model. With a comprehensive model, researchers will be able to evaluate the effects of hundreds of factors on the uniformity of CdS film deposition. Variables such as the temperature, geometry changes, and operating pressures may be altered to discover which parameters have the largest impact on deposition.

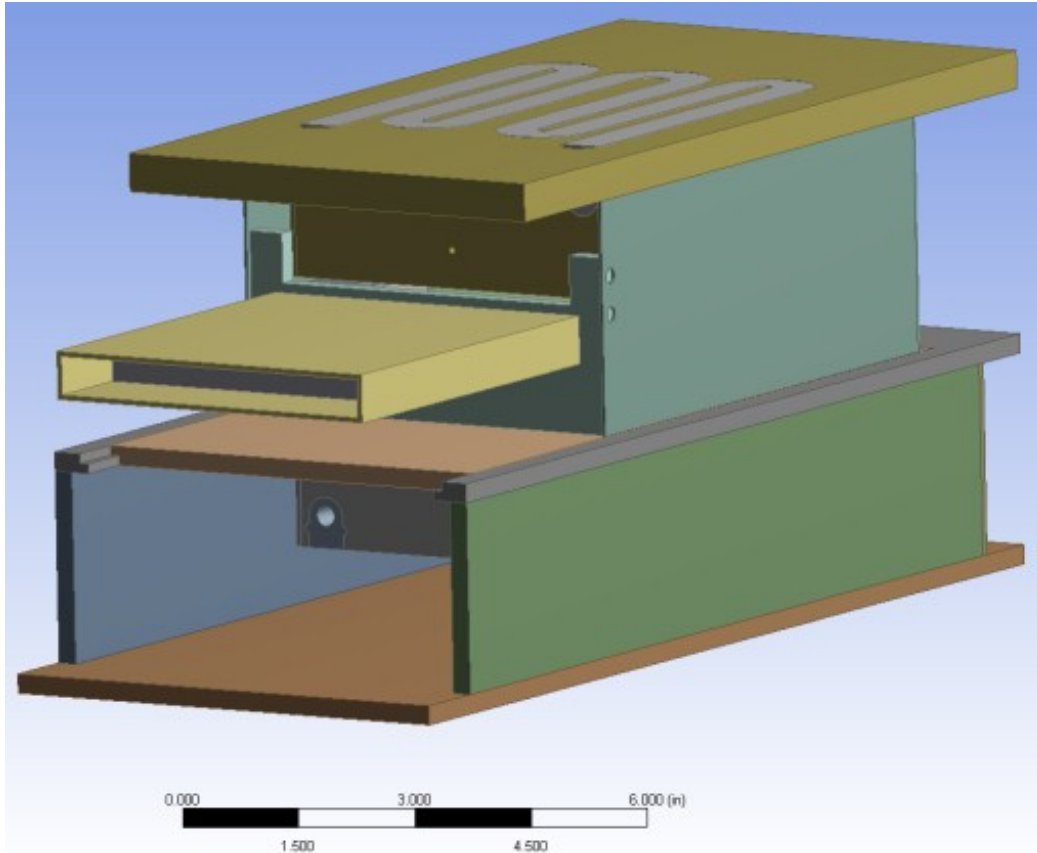


Figure 50. Comprehensive 3D thermal and fluid model: Geometry

### 6.3 *Future Work*

One of the primary goals for this project was to prove that CFD modeling is possible for CSS. As this has been accomplished for the limited experimental cases in which it was attempted, an obvious next step is to validate the model in other experimental conditions before scaling up the developed model for industrial purposes. Experimental validation is needed for several physical phenomena that have been numerically solved for thus far.

The effect of substrate temperature gradients on the film growth has not been adequately observed. A proposed experiment to study this effect is to intentionally create a thermal discrepancy across the substrate. One practical method of doing this would be by heating half of

the substrate before entering the CdS deposition source by placing half of the substrate into the heating station one while keeping the other half in the open chamber. This would ensure that there would be a large thermal gradient between the two halves of the substrate. The film would predictably be thinner on the heated side compared to the cool side, but experimental validation is needed to ensure that the model can accurately handle such a scenario. From these experiments, a design to improve the thermal uniformity of the substrates can be proposed and manufactured.

Further experimental support is also required to validate the precision of the sticking coefficient and the interaction of the fluid with the walls. Though the sticking coefficient remained constant between the normal CdS deposition source and the modified source, it is uncertain whether or not this value is constant with pressure and temperature or if it varies according to some unknown relationship. Many CdS substrates will need to be deposited while sweeping the range of operating pressures and temperatures to observe this relationship.

The same type of verification is needed for the fluid-wall interaction. Though the model fit well with the experimental data, there is a need to somehow isolate and accurately quantify the accuracy of the limited slip assumptions made along the source walls. This type of measurement and analysis would be difficult to accomplish due to the low velocity of flow in the pocket and the intrusiveness of measurement tools in the ARDS.

After validating that the CdS source model is valid for the majority of pressure and temperature operating conditions, this CFD technique may be applied for the other deposition sources. None of the CdTe, CdCl<sub>2</sub>, or CuCl sources have yet been analyzed or optimized in any fashion. As each photovoltaic material has a unique mass, molecular size and flow characteristic, the optimized sources may have completely different geometries. However, much

of the groundwork has been accomplished for the future modeling of other materials with the completed work presented in this thesis. Users need only modify a few coefficients to analyze the other sources. Parameters such as molecular weight, heat transfer coefficients, L-J characteristic lengths, and the Arrhenius rate coefficients must be adjusted for each new element. After these changes are made, it would be possible to simply use the same meshes as developed in this project to model new photovoltaic materials.

## REFERENCES

- [1] C. Wadia, a P. Alivisatos, and D. M. Kammen, “Materials availability expands the opportunity for large-scale photovoltaics deployment.,” *Environmental science & technology*, vol. 43, no. 6, pp. 2072–7, Mar. 2009.
- [2] M. Höök, J. Li, K. Johansson, and S. Snowden, “Growth Rates of Global Energy Systems and Future Outlooks,” *Natural Resources Research*, vol. 21, no. 1, pp. 23–41, Dec. 2011.
- [3] International Energy Agency, “Key World Energy Statistics,” 2012.
- [4] S. Chu and A. Majumdar, “Opportunities and challenges for a sustainable energy future.,” *Nature*, vol. 488, no. 7411, pp. 294–303, Aug. 2012.
- [5] US Energy Information Administration, “Annual Energy Review 2011,” Washington, DC, 2011.
- [6] H. Rogner, “Energy for Development,” vol. 54, pp. 149–160, 2012.
- [7] “Energy ’ s Tricky Tradeoffs,” *Science*, pp. 786–787, 2010.
- [8] US Department of Energy, “SunShot Vision Study,” 2012.
- [9] A. Goetzberger and C. Hebling, “Photovoltaic materials, past, present, future,” *Solar Energy Materials and Solar Cells*, vol. 62, no. 1–2, pp. 1–19, Apr. 2000.
- [10] K. E. Walters, “COMPUTATIONAL FLUID DYNAMICS (CFD) MODELING FOR CdTe SOLAR CELL MANUFACTURING,” 2011.
- [11] A. Goodrich and M. Woodhouse, “PV Manufacturing Cost Analysis: Future Cost Reduction Opportunities,” 2012.
- [12] A. Morales-Acevedo, “Thin film CdS/CdTe solar cells: Research perspectives,” *Solar Energy*, vol. 80, no. 6, pp. 675–681, Jun. 2006.
- [13] W. Mahmood and N. A. Shah, “Study of cadmium sulfide thin films as a window layers,” in *AIP Conf. Proc.*, 2012, vol. 178, no. 1, pp. 178–182.
- [14] N. Duxin, F. Liu, H. Vali, and A. Eisenberg, “Cadmium Sulphide Quantum Dots in Morphologically Tunable Triblock Copolymer Aggregates involved also triblock copolymers such as hydroxylated poly-,” *J. AM. CHEM. SOC.*, no. 18, pp. 392–398, 2005.
- [15] K. Ravichandran and P. Philominathan, “Comparative study on structural and optical properties of CdS films fabricated by three different low-cost techniques,” *Applied Surface Science*, vol. 255, no. 11, pp. 5736–5741, Mar. 2009.

- [16] G. Kazantzis and W. J. Hanbury, "The induction of sarcoma in the rat by cadmium sulphide and by cadmium oxide.," *British journal of cancer*, vol. 20, no. 1, pp. 190–9, Mar. 1966.
- [17] P. Roy and S. K. Srivastava, "A new approach towards the growth of cadmium sulphide thin film by CBD method and its characterization," *Materials Chemistry and Physics*, vol. 95, no. 2–3, pp. 235–241, Feb. 2006.
- [18] J. Torres, J. I. Cisneros, and G. Gordillo, "DETERMINATION OF THE OPTICAL CONSTANTS OF POLICRYSTALLINE CdS," *ADVANCES IN MATERIALS SCIENCE & TECHNOLOGY*, vol. 1, no. 1, pp. 7–12, 2012.
- [19] H. Uda, S. Ikegami, and H. Sonomura, "Structural and Electrical Properties of Chemical-Solution-Deposited CdS Films for Solar Cells," *Japanese Journal of Applied Physics*, vol. 29, no. Part 1, No. 1, pp. 30–33, Jan. 1990.
- [20] A. Bayer, D. S. Boyle, M. R. Heinrich, D. J. Otway, O. Robbe, and P. O'Brien, "Developing environmentally benign routes for semiconductor synthesis: improved approaches to the solution deposition of cadmium sulfide for solar cell applications," *Green Chemistry*, vol. 2, no. 2, pp. 79–86, 2000.
- [21] S. J. C. Irvine, V. Barrioz, A. Stafford, and K. Durose, "Materials issues in very thin film CdTe for photovoltaics," *Thin Solid Films*, vol. 480–481, pp. 76–81, Jun. 2005.
- [22] A. Lopez-Otero, "Hot Wall Epitaxy," *Thin Solid Films*, vol. 49, pp. 3–57, 1978.
- [23] C. a. Menezes, "Low Resistivity CdTe-Te Films by a Combined Hot-Wall-Flash Evaporation Technique," *Journal of The Electrochemical Society*, vol. 127, no. 1, p. 155, 1980.
- [24] S. B. Division, "CdS/CdTe SOLAR CELLS BY THE SCREEN-PRINTING-SINTERING TECHNIQUE: FABRICATION, PHOTOVOLTAIC PROPERTIES AND APPLICATIONS," vol. 23, pp. 89–105, 1988.
- [25] W. Li, R. Ribelin, Y. Mahathongdy, D. Albin, R. Dhere, D. Rose, S. Asher, and H. Moutinho, "The Effect of High-Resistance SnO<sub>2</sub> on CdS / CdTe Device Performance," no. October, 1998.
- [26] H. R. Moutinho, F. S. Haseen, F. Abulfotuh, and L. L. Kazmerski, "Investigation of polycrystalline CdTe thin films deposited by physical vapor deposition, close-spaced sublimation, and sputtering," vol. 13, no. October 1994, pp. 2877–2883, 1995.
- [27] J. Britt and C. Ferekides, "Thin-film CdS/CdTe solar cell with 15.8% efficiency," *Applied Physics Letters*, vol. 62, no. 22, p. 2851, 1993.

- [28] P. D. Paulson and V. Dutta, "Study of in situ CdCl<sub>2</sub> treatment on CSS deposited CdTe @ lms and CdS / CdTe solar cells," vol. 370, pp. 299–306, 2000.
- [29] K. Zweibel, "Issues in thin film PV manufacturing cost reduction," *Solar Energy Materials and Solar Cells*, vol. 59, no. 1–2, pp. 1–18, Sep. 1999.
- [30] K. L. Barth, "Abound Solar's CdTe module manufacturing and product introduction," *2009 34th IEEE Photovoltaic Specialists Conference (PVSC)*, pp. 002264–002268, Jun. 2009.
- [31] D. H. Rose, F. S. Hasoon, R. G. Dhere, D. S. Albin, R. M. Ribelin, X. S. Li, Y. Mahathongdy, T. A. Gessert, and P. Sheldon, "Fabrication procedures and process sensitivities for CdS/CdTe solar cells," *Progress in Photovoltaics: Research and Applications*, vol. 7, no. 5, pp. 331–340, Sep. 1999.
- [32] R. Mendoza-Pérez, J. Sastre-Hernández, G. Contreras-Puente, and O. Vigil-Galán, "CdTe solar cell degradation studies with the use of CdS as the window material," *Solar Energy Materials and Solar Cells*, vol. 93, no. 1, pp. 79–84, Jan. 2009.
- [33] N. Abbas Shah, A. Ali, and A. Maqsood, "Preparation and Characterization of CdTe for Solar Cells, Detectors, and Related Thin-Film Materials," *Journal of Electronic Materials*, vol. 37, no. 2, pp. 145–151, Nov. 2007.
- [34] A. Luque and A. Mart, *Theoretical Limits of Photovoltaic Conversion*. 2003.
- [35] S. N. Alamri, "The growth of CdTe thin film by close space sublimation system," *Physica Status Solidi A*, vol. 200, no. 2, pp. 352–360, Dec. 2003.
- [36] J. L. Cruz-Campa and D. Zubia, "CdTe thin film growth model under CSS conditions," *Solar Energy Materials and Solar Cells*, vol. 93, no. 1, pp. 15–18, Jan. 2009.
- [37] V. Sosa, R. Castro, and J. L. Pena, "Pressure and temperature influence on CdTe thin-film deposit by close-spaced vapor transport technique," *Journal of Vacuum Science & Technology A: Vacuum, Surfaces, and Films*, vol. 8, no. 2, pp. 979–983, 1990.
- [38] S. W. Kim and G. H. Kim, "Thickness-profile measurement of transparent thin-film layers by white-light scanning interferometry.," *Applied optics*, vol. 38, no. 28, pp. 5968–73, Oct. 1999.
- [39] L. Deck and P. De Groot, "High-speed non-contact profiler based on scanning white light interferometry," *Int. J. Mach. Tools Manufact.*, vol. 35, no. 2, pp. 147–150, 1995.
- [40] P. Sandoz, "Wavelet transform as a processing tool in white-light interferometry.," *Optics letters*, vol. 22, no. 14, pp. 1065–7, Jul. 1997.

- [41] Y.-S. Ghim and S.-W. Kim, "Thin-film thickness profile and its refractive index measurements by dispersive white-light interferometry.," *Optics express*, vol. 14, no. 24, pp. 11885–91, Nov. 2006.
- [42] J. Anderson, *Computational fluid dynamics*, Third. 1995.
- [43] H. Lomax, T. Pulliam, D. Zingg, and T. Kowalewski, "Fundamentals of Computational Fluid Dynamics," *Applied Mechanics Reviews*, vol. 55, no. 4, p. B61, 2002.
- [44] Y. K. Chae, "Chemical Vapor Deposition Reactor Design Using Small-Scale Diagnostic Experiments Combined with Computational Fluid Dynamics Simulations," *Journal of The Electrochemical Society*, vol. 146, no. 5, p. 1780, 1999.
- [45] P. K. Kundu and I. M. Cohen, *Fluid Mechanics*, Second. San Diego: Academic Press, 2002, p. 119.
- [46] H. Struchtrup, *Macroscopic Transport Equations for Rarefied Gas Flows*. Berlin/Heidelberg: Springer-Verlag, 2005.
- [47] E. Rabani, "An interatomic pair potential for cadmium selenide," *The Journal of Chemical Physics*, vol. 116, no. 1, p. 258, 2002.
- [48] W. L. Jorgensen, "Intermolecular Potential Functions and Monte Carlo Simulations for Liquid Sulfur Compounds," *J. Phys. Chem.*, vol. 90, pp. 6379–6388, 1986.
- [49] C. Housiadas, Y. Drossinos, and F. E. Larrode, "Slip-flow heat transfer in circular tubes," *International Journal of Heat and Mass Transfer*, vol. 43, pp. 2669–2680, 2000.
- [50] H. Yamaguchi, Y. Matsuda, and T. Niimi, "Tangential Momentum Accommodation Coefficient measurements for various materials and gas species," *Journal of Physics: Conference Series*, vol. 362, p. 012035, May 2012.
- [51] J. H. I. Lienhard and J. H. V Lienhard, *A heat transfer textbook*, 4th Editio., vol. 82, no. 1. Cambridge, MA: Phlogiston Press, 2012.
- [52] ANSYS, "ANSYS FLUENT Theory Guide," vol. 15317, no. 13.0. ANSYS, Inc., Canonsburg, PA, 2010.
- [53] R. Siegel and J. R. Howell, *THERMAL RADIATION HEAT TRANSFER Volume III: Radiation Transfer With Absorbing, Emitting, and Scattering Media*, vol. III. Washington, D.C.: U.S. Government Printing Office, 1971.
- [54] C. Su, "GROWTH RATE OF CdS BY VAPOR TRANSPORT IN A CLOSED AMPOULE Ching-Hua SU," vol. 80, pp. 333–342, 1987.

- [55] C. Hongjuan, X. Yongkuan, Y. Wei, Y. Xianglu, Y. Ruyue, and L. Zhanping, "Growth of CdS crystals by the physical vapor transport method," *Journal of Semiconductors*, vol. 30, no. 10, p. 103002, Oct. 2009.
- [56] T. S. Jeong, C. I. Lee, P. Y. Yu, Y. J. Shin, H. K. Shin, T. S. Kim, H. Lee, J. Y. Kim, and K. J. Hong, "Growth of cadmium sulfide single crystal by the sublimation method," *Journal of Crystal Growth*, vol. 155, no. 1–2, pp. 32–37, Oct. 1995.
- [57] C. L. Yaws and R. W. Pike, *YAWS HANDBOOK OF ANTOINE COEFFICIENTS FOR VAPOR PRESSURE 2nd ELECTRONIC EDITION*. 2009.
- [58] V. D. Falcão, W. A. Pinheiro, C. L. Ferreira, L. Rosa, D. O. Cruz, I. M. De Engenharia, D. De Engenharia, and L. D. F. Finos, "Influence of Deposition Parameters on the Properties of CdTe Films Deposited by Close Spaced Sublimation 3 . Results and Discussion," vol. 9, no. 1, pp. 29–32, 2006.
- [59] F. Kaldis, "CRYSTAL GROWTH AND GROWTH RATES OF CdS BY SUBLIMATION AND CHEMICAL TRANSPORT," *Journal of Crystal Growth*, vol. 5, pp. 376–390, 1969.
- [60] M. M. Faktor, I. Garrett, R. Hecklngbottom, and D. Hill, "DIFFUSIONAL LIMITATIONS IN GAS PHASE GROWTH OF CRYSTALS," vol. 9, pp. 3–11, 1971.
- [61] G. a. Somorjai and D. W. Jepsen, "Evaporation Mechanism of CdS Single Crystals. I. Surface Concentration and Temperature Dependence of the Evaporation Rate," *The Journal of Chemical Physics*, vol. 41, no. 5, p. 1389, 1964.
- [62] I. M. De Schepper, H. Van Beyeren, and M. H. Ernst, "The nonexistence of the linear diffusion equation beyond Fick's law," *Physica*, vol. 75, no. 1, pp. 1–36, Jul. 1974.